A Framework for Analysis of the Uncertainty of Socioeconomic Growth and Climate Change on the Risk of Water Stress: a Case Study in Asia

Charles Fant, C. Adam Schlosser, Xiang Gao,
Kenneth Strzepek and John Reilly

MIT JOINT PROGRAM ON THE SCIENCE AND POLICY of GLOBAL CHANGE

Report No. 269
November 2014

The MIT Joint Program on the Science and Policy of Global Change combines cutting-edge scientific research with independent policy analysis to provide a solid foundation for the public and private decisions needed to mitigate and adapt to unavoidable global environmental changes. Being data-driven, the Program uses extensive Earth system and economic data and models to produce quantitative analysis and predictions of the risks of climate change and the challenges of limiting human influence on the environment—essential knowledge for the international dialogue toward a global response to climate change.

To this end, the Program brings together an interdisciplinary group from two established MIT research centers: the Center for Global Change Science (CGCS) and the Center for Energy and Environmental Policy Research (CEEPR). These two centers—along with collaborators from the Marine Biology Laboratory (MBL) at Woods Hole and short- and long-term visitors—provide the united vision needed to solve global challenges.

At the heart of much of the Program's work lies MIT's Integrated Global System Model. Through this integrated model, the Program seeks to: discover new interactions among natural and human climate system components; objectively assess uncertainty in economic and climate projections; critically and quantitatively analyze environmental management and policy proposals; understand complex connections among the many forces that will shape our future; and improve methods to model, monitor and verify greenhouse gas emissions and climatic impacts.

This reprint is one of a series intended to communicate research results and improve public understanding of global environment and energy challenges, thereby contributing to informed debate about climate change and the economic and social implications of policy alternatives.

Ronald G. Prinn and John M. Reilly,
Program Co-Directors

For more information, contact the Program office:
MIT Joint Program on the Science and Policy of Global Change

Postal Address:
Massachusetts Institute of Technology
77 Massachusetts Avenue, E19-411
Cambridge, MA 02139 (USA)

Location:
Building E19, Room 411
400 Main Street, Cambridge

Access:
Tel: (617) 253-7492
Fax: (617) 253-9845
Email: ***globalchange@mit.edu***
Website: ***http://globalchange.mit.edu/***

A Framework for Analysis of the Uncertainty of Socioeconomic Growth and Climate Change on the Risk of Water Stress: a Case Study in Asia

Charles Fant[*†], C. Adam Schlosser[*], Xiang Gao[*], Kenneth Strzepek[*] and John Reilly[*]

Abstract

The sustainability of future water resources is of paramount importance and is affected by many factors, including population, wealth and climate. Inherent in how these factors change in the future is the uncertainty of their prediction. In this study, we integrate a large ensemble of scenarios—internally consistent across economics, emissions, climate, and population—to develop a risk portfolio of water stress over a large portion of Asia that includes China, India, and Mainland Southeast Asia. We isolate the effects of socioeconomic growth from the effects of climate change in order to identify the primary drivers of stress on water resources. We find that water needs related to socioeconomic changes, which are currently small, are likely to increase considerably in the future, often overshadowing the effect of climate change on levels of water stress. As a result, there is a high risk of severe water stress in densely populated watersheds by 2050, compared to recent history. If socio-economic growth is unconstrained by global actions to limit greenhouse gas concentrations, water-stressed populations may increase from about 800 million to 1.7 billion in this region.

Contents

[*] Joint Program on the Science and Policy of Global Change, Massachusetts Institute of Technology, MA, USA.
[†] Corresponding author (Email: chasfant@mit.edu)

1. INTRODUCTION

There is rising concern about the impact of climate change and socioeconomic growth on the future of our water resources (e.g., Jiménez Cisneros *et al.,* 2014; Georgakakos, 2014). The global climate system and population as well as the local and global economy determine regional and local water supplies and demands—and these forces can result in complex interactions that require deeper understanding in order to provide actionable information to stakeholders for strategic planning in a changing and growing world. An emerging need is evident for modeling tools to capture these complex linkages—especially global-to-local hydro-climatic relationships, managed water systems, and population and economic growth.

Previous literature has included many assessments of the impacts of climatic changes and socioeconomic drivers on water supply and demand (Alcamo *et al.,* 2007, 2010; Arnell *et al.,* 2011; Shen *et al.,* 2008; Vörösmarty *et al.,* 2000; among others). These studies have focused on a limited number of future scenarios, providing valuable insights on the potential changes that may arise from a few plausible futures; however, there is no ability to assess where these courses of events and the subsequent water impacts may lie in terms of a distribution of outcomes—i.e. a risk-based lens to the analyses. Given the complexity of the system, critical questions remain such as:

- For any scenario of future climate, population and economy, can we identify a central tendency as well as the "extreme" outliers (i.e. 5th and 95th percentile)?
- Does any scenario result cluster around a central tendency or mode, and therefore indicate that the outcome is more robust?

Without quantified likelihoods of future outcomes, it is difficult to determine which scenarios should be seriously considered when planning new investments. Here we develop and test an approach to provide regional projections of changes in water supply and demand, and of the potential for changes in water stress.

We draw on probabilistic projections of global population, economic growth, emissions and climate developed using an Integrated Global Systems Model (IGSM) developed at MIT (Sokolov, *et al.*, 2009; Webster *et al.*, 2012). Advantages of this approach are (1) likelihoods are explicitly quantified; (2) scenarios are self-consistent, in that a climate scenario drawn from these projections was produced from an emissions scenario driven by an associated population and economic growth scenario (recoverable for our projection of water demands and resource uncertainty); (3) underlying uncertainties in drivers of both economic and earth system response are sampled; (4) cascading uncertainties are properly addressed, while additional uncertain variables increase uncertainty in final outcomes, unless the underlying parametric uncertainties are highly correlated (in which case they have a strong tendency to offset one another).

To test the approach we focus on a portion of Asia that includes China, India and Mainland Southeast Asia (**Figure 1**). This region covers emerging economies constituting almost half of today's global population, as well as diverse climates that create varied water resource issues involving both surface and ground water. Previous studies in this region have found moderate

effects of climate change, some positive and some negative, but raise serious concerns about socioeconomic effects on water-intensive economic sectors (Wei *et al.* 2009; Piao *et al.,* 2010; O'Brien *et al.,* 2004; Kumar *et al.* 2006). These regional studies, like the previously mentioned global studies, are constrained to a limited number of climatic and socioeconomic scenarios provided by Climate Model Intercomparison Projects (CMIPs) and the Intergovernmental Panel on Climate Change (IPCC).

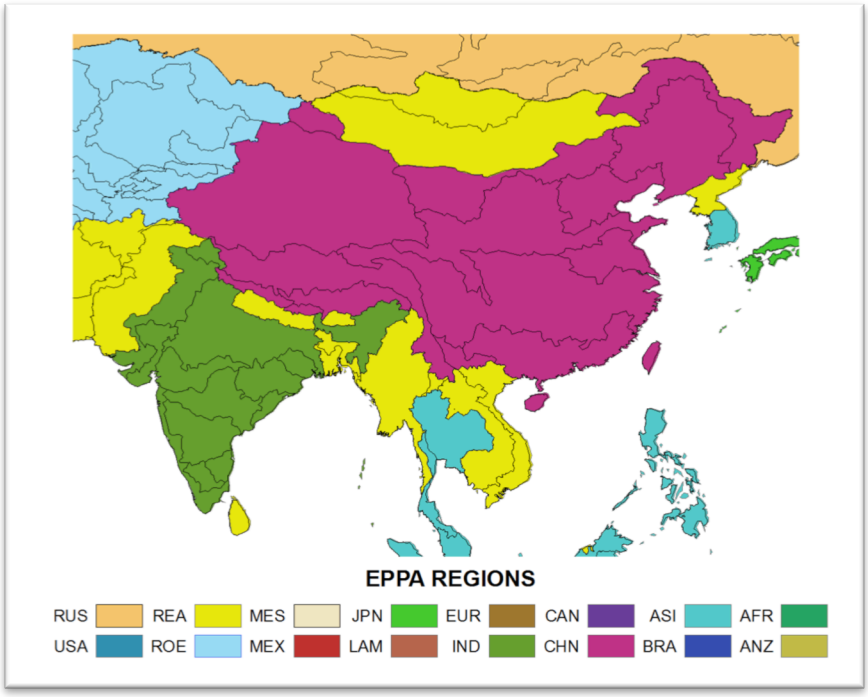

Figure 1. Southeast Asia study region. Black contours delineate Assessment Sub Regions (ASRs) defined for the Water Resource System (WRS) within the IGSM-WRS framework. The color shading indicates the economic regions that are resolved in the Emissions Prediction and Policy Analysis (EPPA) model.

Our method, in brief, is to apply a Water Resource System (WRS) model developed to work with the IGSM framework (Strzepek *et al.* 2013). We use 400-member ensembles of climate forecasts previously developed with the IGSM (Sokolov, *et al.*, 2009; Webster *et al.*, 2012), complemented with the pattern-scaling approach of Schlosser *et al.* (2012) to develop a new 6,800-member ensemble of climate change projections, including variations in the regional pattern of climate change as represented by major General Circulation Models (GCMs). The climate projections drive changes in surface water supply through changes in runoff and irrigation demand, and the IGSM economic ensemble projections provide the necessary parameters to estimate changes in water demands for industry and municipal use. A water management module within the WRS allocates, stores and releases water over each year, regulated by a management decision scheme that sets priorities among uses. This allows a distribution of water stress, indicating risks for river basins and sub-basins within our target region of Asia.

In Section 2 of this paper, the models and methods are described; in Section 3, the changes in water supply and demand are shown in detail, as well as the resulting water stress risk portfolios; and in Section 4, the main conclusions from this work are presented.

2. MODELS AND METHODS

2.1 The IGSM-WRS and Study Region

Our analysis focuses on the impact of socioeconomic growth and climate changes on the future availability and management of water resources resolved over large watersheds—Assessment Study Regions (ASRs)—across South, Southeast, and East Asia (Figure 1). The basic structure of the WRS as applied here is illustrated in **Figure 2**, with greater detail provided in Strzepek *et al.* (2013).

The WRS is driven by economic and climatic projections from the MIT Integrated Global System Model (IGSM) described in Sokolov *et al.* (2005). Economic projections are driven by the MIT Economic Projection and Policy Analysis (EPPA) model, a regionally resolved general equilibrium model of world economies (described in Paltsev *et al.* (2005)), which provides inputs for econometrically estimated relationships of industrial and municipal water requirements based on changes in population and gross domestic product (GDP) (Strzepek, *et al.*, 2013).

The same EPPA scenarios provide greenhouse gas and other pollutant emissions to the MIT Earth System Model (MESM), which produces latitudinally-resolved climate projections; the IGSM sub-model of atmospheric dynamics and chemistry is 2-dimensional (altitude and latitude) and is coupled to a mixed layer ocean component. The zonal resolution of the MESM makes it feasible to produce 400-member ensembles necessary to reasonably resolve the distribution of future climate outcomes (Webster *et al.*, 2012). MESM outputs are downscaled to 2° latitude by 2.5° longitude using a pattern-scaling technique (Schlosser *et al.*, 2012) based on archived IPCC4 Climate model simulations. These downscaled precipitation and temperature results are used to drive the Community Land Model (CLM) version 3.5 (Oleson *et al.*, 2008) to produce the runoff for each ASR. The CLM, which explicitly represents soil thermal and hydrologic processes, is also implemented within the IGSM as its land surface scheme. The simulated runoff is further refined through a calibration procedure (Strzepek *et al.*, 2013) to ensure that projected flows in each basin are a realistic representation of natural flow conditions.

Downscaled precipitation and temperature are also input to the CliCrop component of the WRS, a daily crop water deficit model which projects irrigation requirement (Fant *et al.,* 2012). The multiple water demands are inputs to the Water System Management (WSM) component of the WRS that allocates water for consumption and assesses the adequacy of water supplies in light of changing water availability at the ASR level. We use previously published and archived ensemble IGSM runs that consider underlying uncertainty in both climatic (climate sensitivity, ocean uptake and aerosol effects) and economic parameters (labor and energy productivity growth, population, resource availability, technology costs, pollution emissions and substitution elasticities) as described in Webster *et al.* (2012).

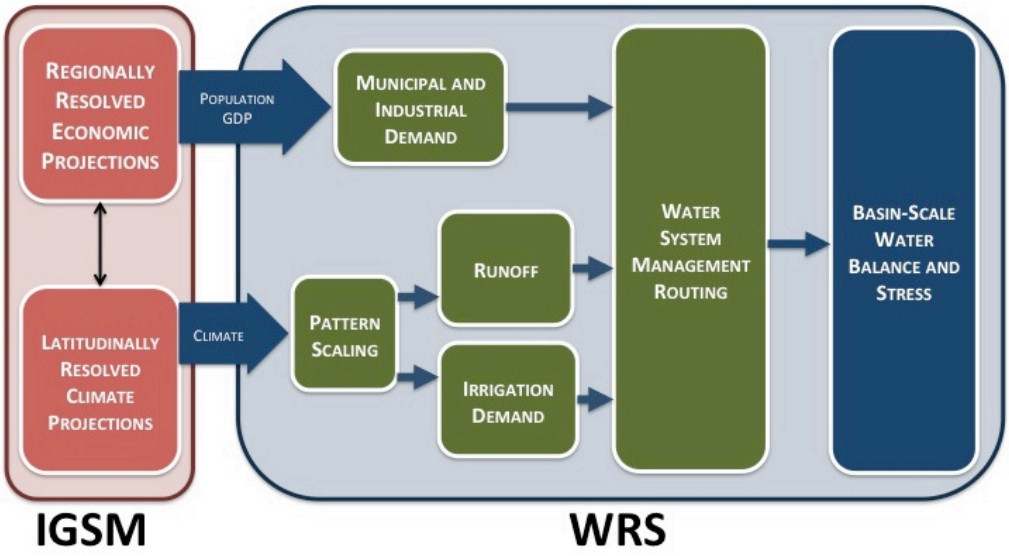

Figure 2. Schematic of connections between components of the IGSM framework and the WRS. Within the IGSM, the EPPA model produces economic projections, calculating population and GDP for each ASR. These determine municipal and industrial demands for water. Climate results from MESM are projected longitudinally via pattern scaling with archived GCM data. CLM determines runoff, and CliCrop calculates irrigation demands. Water demands and surface-water supply are fed into the WSM to optimize the routing of water across all ASRs. The resultant routing is then analyzed via water stress indicators.

For this study, the WRS is configured to represent 54 ASRs over a large region of Asia (see Figure 1). The ASRs are defined by major river basins and parts of river basins contained within a country.[2] For each ASR, available reservoirs are aggregated into a single storage unit that receives water from runoff within the ASR and remaining flows of upstream ASRs. The stored water is allocated to serve human water sector requirements and a required environmental flow. Non-irrigation requirements (for municipal, industrial, and livestock uses) are driven by socioeconomic factors on the assumption they are not significantly influenced by climate; irrigation requirements, on the other hand, are determined by environmental conditions, calculated by CliCrop (Fant *et al.,* 2012).

Based on recent evidence over the past decade, global growth in irrigated land area has slowed considerably (e.g. Siebert *et al.*, 2013; Thenkabail *et al.*, 2008; and Siebert *et al.*, 2005) even though global food production has steadily increased (e.g. FAO, 2013). This indicates that rising global food demand is being met by increased rainfed agriculture and intensification of existing irrigated land. Given the complexity of interactive socio-economic drivers and environmental pressures, as well as global and national governance that will affect future decisions regarding irrigation expansion (i.e. new dams and reservoirs, e.g. WCOD, 2000), the irrigated area is held constant in these experimental simulations (equal to current estimates from FAO and IFPRI—see Rosegrant *et al.*, 2008); we focus on whether there is adequate water to meet needs associated with changes in ASR-scale socio-economic activity and climate.

[2] A comprehensive ASR listing is provided in Strzepek *et al.* (2013) as well as the basin-level processes of the natural and managed water system that are represented by the model.

2.2 Ensemble Simulations and Scenarios

Our method is to construct numerous ensembles that incorporate the uncertainty in future hydrology and water resources, as affected by uncertainty in climate and economic drivers of water use. We gauge the changes simulated in these ensembles with respect to a single baseline scenario. The baseline scenario represents a 50-year IGSM run with year-2000 water needs from agriculture, industry, and municipalities and a mean year-2000 climate with 50 years of recent historical inter-annual climate variability. We compare resulting changes in supply, demand, or water stress with the baseline result to isolate the effect of the long-term mean change in climate. For baseline domestic and industrial water requirements, we use data from Rosegrant *et al.* (2008) that are also used in the global IGSM-WRS, described in detail in Strzepek *et al.* (2013).

Our projections are designed to distinguish effects on water use of economic and population growth separate from that of future climate change. We create three ensembles of 50-year simulations (2000–2050) of water resource supply and use. In the first, we utilize forecasts of the socioeconomic drivers of water demand to create an ensemble as if only the economy changed (no climate change), which we hereafter refer to as the *Just Growth* ensemble. In the second, we utilize the same economic scenarios and associated emissions, simulating their effect on climate to create another ensemble as if only the climate changed, which we hereafter label the *Just Climate* ensemble. Finally, we develop a large ensemble including both climate change and economic growth, which we hereafter label the *Climate and Growth* ensemble. These ensembles allow us to separately identify the relative importance of climate change and growth, study the combined effect of these changes, and compare them against a baseline ensemble (as if neither climate nor socio-economic drivers changed). The *Just Growth*, *Just Climate*, and *Climate and Growth* ensembles are all generated on the assumption that there are no policy constraints on greenhouse gas emissions. Analyzing mitigation effects in this region will be handled in a future study.

2.2.1 Baseline Scenario Data

A long-term, globally consistent dataset of near-surface meteorological variables—the Global Meteorological Forcing Dataset (GMFD) (Sheffield *et al.*, 2006)—provides the baseline climate in this study. The data is constructed by combining a suite of global observation-based datasets with the National Centers for Environmental Prediction-National Center for Atmospheric Research (NCEP-NCAR) reanalysis. The GMFD data spans the years 1948 to 2008 at the 1° spatial and 3-hourly temporal resolution.

To detrend the 3-hourly forcing, the data is aggregated monthly, then regridded to a 2.5° × 2° resolution. The linear trend is estimated for each of twelve months at each grid over our study region based on the 50-year (1951–2000) monthly time series. Six near-surface meteorological variables have been processed, including 2 m air temperature, total precipitation, shortwave and longwave radiation, wind speed, and specific humidity. To bridge the potential gaps between the detrended baseline climate in the last year and the derived future climate (discussed in the following section) at the beginning of the future simulations, for each of the twelve months, we add the fitted trend in the last year (Year 2000) to the monthly residual across the 50-year, then

calculate the ratio of this sum to the aggregated monthly time series. The detrended 3-hourly data at each grid are then obtained by scaling the original 3-hourly time series with this monthly ratio. Note that the same ratio is applied across each of the 3-hourly time steps within a specific month. The CLM is then forced with the detrended 3-hourly near-surface meteorological forcing to produce the baseline monthly runoff.

2.2.2 Climate Change and Growth Scenario Data

This study considers changes in GDP and population obtained in the unconstrained emissions (UCE) ensemble analyzed by Sokolov *et al.* (2005). The UCE policy uses the global ensemble of population projections described in Webster *et al.* (2008). To be consistent with the IGSM uncertainty formulation, socioeconomic projections are provided by EPPA region (Figure 2). To provide these population projections at the ASR scale, the EPPA regions' rate of population changes are mapped to the ASR regions within each EPPA region, following the technique used in Strzepek *et al.* (2013). ASR-based population projections use the growth rates from EPPA, with the current populations at the ASR level developed by IPFRI (Rosegrant *et al.,* 2008) (**Figure 3**).

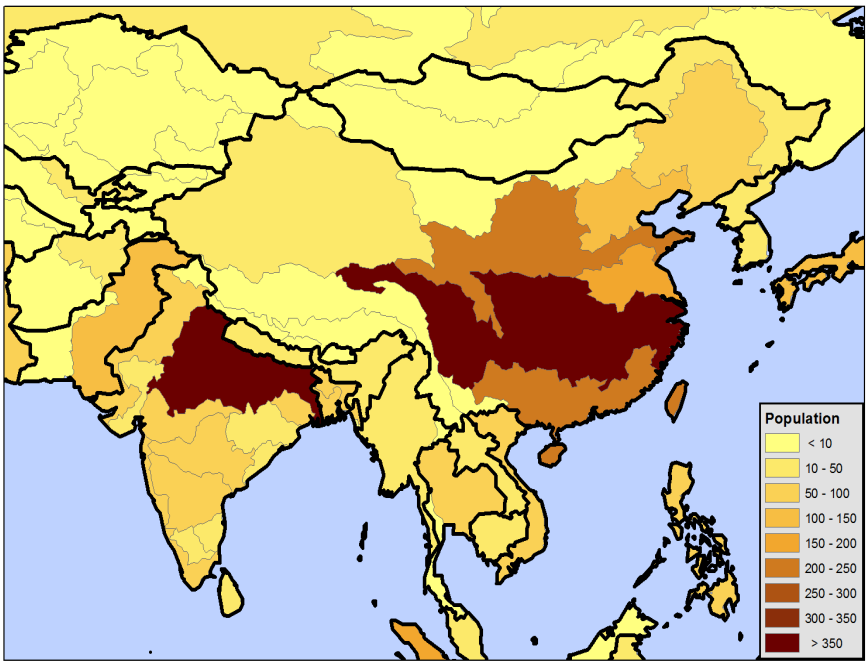

Figure 3. Year 2000 global distribution of population (in millions) projected onto the Assessment Sub Regions (ASRs) of the WRS water-management network of river basins. Black contours denote political boundaries.

The MIT IGSM is designed to quantify various sources of uncertainty in climate projections. The fully coupled IGSM is forced from 1861 to 1990 by observed changes in greenhouse gas concentrations, and from 1991 to 2100 by emissions of greenhouse gas and aerosol precursors projected by the EPPA model (Sokolov *et al.*, 2009). Our 400-member climate forecast ensemble was conducted based on different value combinations of three key climate parameters: effective

climate sensitivity, ocean heat uptake rate, and net aerosol forcing (Sokolov *et al.*, 2009). The value of each parameter is sampled from its probability distribution obtained by comparing the twentieth-century simulations with observations of surface, upper-air, and deep-ocean temperature changes (Forest *et al.,* 2008). The climate forecast ensemble is calculated for each of five emission pathways: Unconstrained Emissions (*No Policy*) and four greenhouse-gas stabilization levels (*Level 1, Level 2,* etc.). In this study, only the results for Unconstrained Emissions are presented.

In the assessment of regional climate change impact on water resource management in Southeast Asia, we use a simple downscaling method, or delta method (Ramirez-Villegas and Jarvis, 2010), to construct a series of atmospheric forcing to conduct our ensemble simulations. The method is based on applying the interpolated monotonic changes in climate from the IGSM projections to the baseline climate, accounting for any bias (or trend) in the baseline climate under future climate change. This method assumes that changes in climates (anomalies) are mostly relevant in the IGSM projections, and that the relationships between variables in the baseline climate—including periodic and irregular fluctuations in variables—are likely to be maintained. The zonal anomalies (delta) are derived for the IGSM monthly time series of 2001 to 2100 with respect to the 20-year (1981–2000) climatology for each meteorological variable and each of the 400 climate forecast scenarios. There exist some biases in the IGSM-simulated zonal precipitation of potential climate change, and we correct such biases based on the monthly zonal precipitation climatology of three periods (2011–2040, 2041–2070, 2071–2100) from the SRESA2 simulation of the Intergovernmental Panel on Climate Change (IPCC) 4th Assessment Report (AR4) (Meehl *et al.*, 2007). The monthly zonal precipitation climatology from each of the 17 GCMs in the SRESA2 scenario has been analyzed to examine the impact of model structure in bias correction.

To account for the uncertainty in regional climate change, a downscaling technique (Schlosser *et al.*, 2012) is employed to expand the IGSM monthly zonal anomalies of precipitation and 2 m air temperature of each of 400 climate forecast scenarios across longitude at 2.5° × 2° by applying longitudinally-resolved patterns, from observations and from climate model projections archived for the IPCC AR4. The observed patterns for precipitation and temperature are derived from the 31-year (1979–2009) monthly GPCP v2.1 data set (Huffman *et al.*, 2009) and the 20-year (1981–2000) monthly Princeton data set, respectively. The pattern shifts in response to human-forced change are derived based on the same 17 GCM simulations from the IPCC AR4 SRESA2 emission scenario. The resulting meta-ensemble (400 × 17 = 6,800 members) of the 2.5° × 2° IGSM monthly anomalies (precipitation and temperature) is used for the Gaussian quadrature procedure presented later.

The IGSM monthly zonal anomalies of each climate forecast scenario are further interpolated using a polynomial of degree 3, with a least-squares fit, to produce a smooth time series (removing rapid changes in gradient in the vicinity of the data points). This is performed for all the near-surface meteorological variables, except that the zonal precipitation anomalies go through the additional bias correction (as described before) prior to the interpolation procedure.

A similar downscaling technique (Schlosser *et al*., 2012) is used to map the interpolated IGSM monthly climate across longitude. These anomalies are then added to the detrended 3-hourly baseline climate to construct the future 3-hourly atmospheric forcing (so called "delta method"), which is used to drive the CLM offline from 2001 to 2050 to simulate the runoff for the subset of 6,800 meta-ensemble members.

The combined effect of growth and climate are then explored in combination through WSM. The IGSM-WRS is integrated to 2050 for all cases. The following analyses will focus on the ability of the ASRs to meet water demands (Strzepek *et al.*, 2013), and the relative stress that these demands place on renewable surface water and water available within the managed system.

2.3 Ensemble Thinning via Gaussian Quadrature Procedure

Due to computational limitations, running the full ensemble of 6,800 members is infeasible. For this reason, we use a Gaussian Quadrature approach, as described in Arndt *et al.* (2014), to produce a subset and respective weights that represent the full ensemble. The Gaussian Quadrature approach identifies a set of indices for the ensemble members, and then identifies a subsample of simulations for which the values of the identified indices are distributed similarly to that of the full ensemble. Thus, we select a series of indices—or summary statistics—that characterize relevant differences among the ensemble members. The number of statistics used determines the size of the resulting subset (i.e., more statistics results in a larger subset) related to the number of equations to solve in order to obtain the Gaussian Quadrature (originally proven in Tchakaloff (1957)), with more detail for the specific application in Arndt, *et al.* (2014).

Two key impacts on water resources are runoff (an indicator of water supply) and irrigation demand. These impacts integrate many aspects of different climate scenarios including precipitation and Potential Evapotranspiration (PET). Willmott and Feddema (1992) developed the Climate Moisture Index (CMI), which uses the ratio of annual precipitation (*P*) to annual PET as follows:

$CMI = (P/PET) - 1$ when $P < PET$

$CMI = 1 - (PET/P)$ when $P >= PET$

CMI may range from +1 to -1, with wet climates showing positive CMI, and dry climates negative CMI. Strzepek *et al.* (2011) demonstrated that changes in CMI are highly correlated with changes in runoff and irrigation demand. Thus, CMI is a single, simple to calculate index that is highly correlated with major impacts of interest in this study.

We calculated CMI for each of the 6,800 climates for 5 regions based on the Koeppen-Geyger climatic zones (shown in **Figure 4Error! Reference source not found.**) and for two 5-year time slices: a mean over 2028 to 2032 and a mean over 2046 to 2050. In the CMI calculation, we use the modified Hargreaves equation to calculate PET (Hargreaves and Allen, 2003). Since WRS also accounts for changes to GDP and population, we add four more indices: year 2050 GDP and population for both India and China. This leaves us with 14 indices total: 10 for climate (5 regions over 2 time slices) and 4 for socioeconomics.

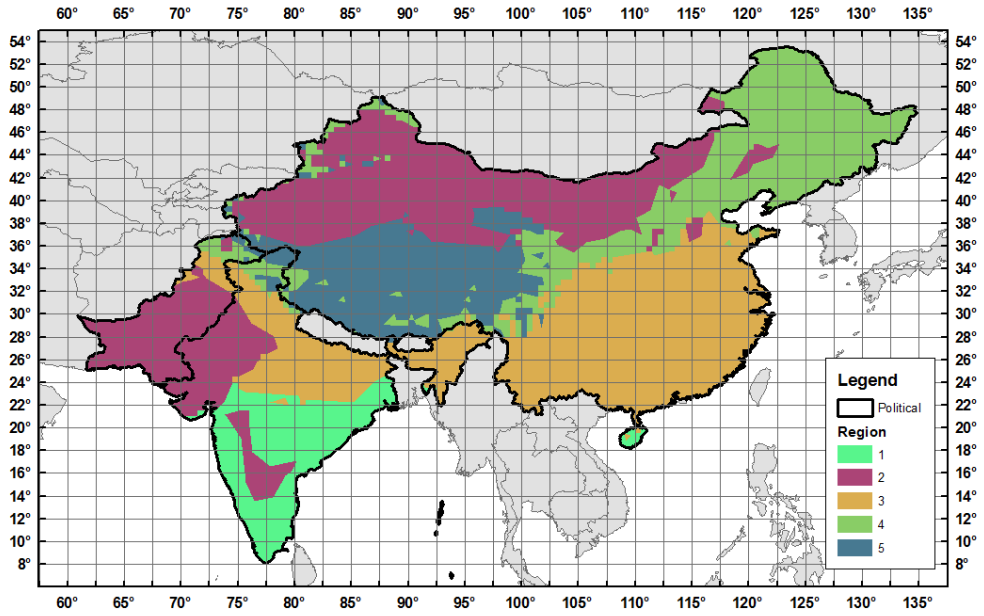

Figure 4. Regions used in the Gaussian Quadrature summary statistics with 2.5° longitude by 2.0° latitude HFD grids. Colored polygons denote the 5 regions used for the Gaussian Quadrature thinning, based on the Koeppen-Geyger Climatic Zones. Black lines are the political boundaries of China, India, and Pakistan.

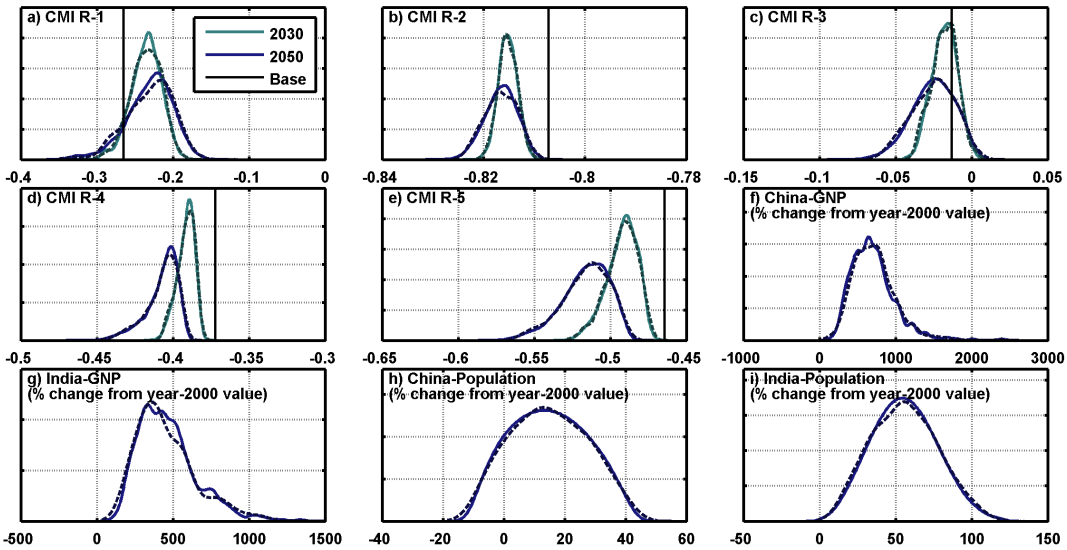

Figure 4. Distribution of the 14 Climate Moisture Index (CMI) statistics used in the Gaussian Quadrature thinning procedure across climate scenarios for the full 6,800-member ensemble. Dashed lines are the Gaussian Quadrature subset distributions for comparison.

Figure 4 shows the distribution of the 14 variables for the full ensemble. In this figure, plots a) through e) show the CMI of the 5 regions for the two time slices. In these CMI plots, the dark black line marks the base CMI value. Plots f) and g) show GDP for China and India in 2050 as a percent change from the year-2000 value, and plots h) and i) show population for China and India in 2050, also as a percent change from the year-2000 value. The distributions of the resulting subset are shown as dashed lines. As shown, the Gaussian Quadrature procedure

successfully reproduces the original 6,800 member ensemble with a sub-sampled set of 551 members. We then use this sub-sampled ensemble to perform our water resource assessment.

2.4 Measures of Water Stress

We use two measures of stress to understand the impacts of changes in climate and growth. The first measure, Unmet Water Requirement (UWR), is the percentage of the total water requirement that is not met by the system. UWR is the main component of the objective function in WSM and is a direct aggregate measure of water stress in each ASR. We calculate UWR as follows:

$$UWR = \left(1 - \frac{total\ water\ consumption}{total\ water\ requirement}\right) \times 100\%$$

In the global WRS model, total water requirement is an estimate of the amount of water that would be consumed given socio-economic factors, climate conditions, and current infrastructure, if water were an unlimited resource. For example, if the total water requirement—irrigation, industrial, and municipal—is 100 billion cubic meters (BCM) and the system can only deliver 90 BCM, the UWR would be 10%. A UWR of 0% indicates that all crops (as well as the other water requirement sectors) are without water stress. The WSM module allocates domestic and industrial consumption requirements to be satisfied first (given sufficient water supply) and the agriculture sector must absorb the loss. Since irrigation is by far the highest requirement for water, it is extremely rare that domestic and industrial sectors absorb any loss from the water limitations. Furthermore, since crops are irrigated depending on their value and water availability, many crops are partially irrigated on a regular basis, which is why we see unmet requirement in the baseline scenario (see **Figure 5**). Partial irrigation complicates the interpretation of UWR in the baseline scenario, so we focus on changes in UWR, assuming that these changes indicate additional stress in a given region. For instance, an increase in unmet requirement would likely decrease the supply from the agriculture sector, which could increase food prices.

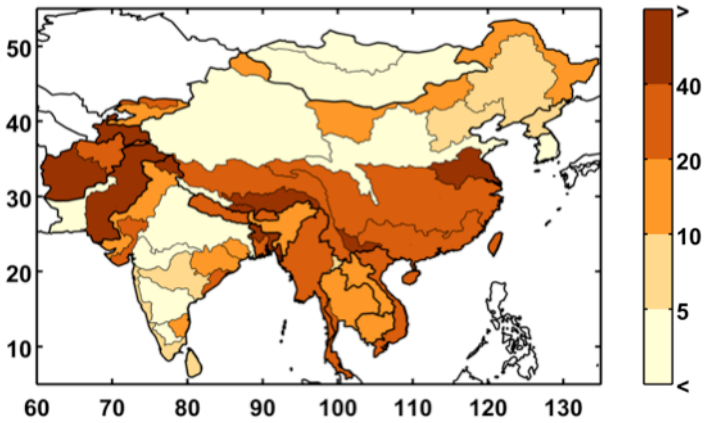

Figure 5. Baseline unmet water requirement (%) for the study region at the ASR level. Unmet requirement is defined as total consumptive use divided by the total water requirement.

The second measure, a Water Stress Index (WSI), is used to assess the stress on the water resource system for each ASR. For this, we use the metrics adopted for other applications of the

IGSM-WRS (Strzepek *et al.*, 2013; Blanc *et al.*, 2013). Our WSI, similar to that developed by Smakhtin *et al.* (2005), is based on input water flows (from surface runoff and upstream ASRs) and desired withdrawals, as a measure of the pressure that human water uses exert on renewable surface fresh water. This measure does not calculate unmet requirement; instead, it gauges stress on the natural water system through its accounting for withdrawal and consumptive uses. WSI is calculated as the ratio of each ASR's mean annual total withdrawal (*TW*), which by definition includes consumptive loss, to the mean annual runoff (*RUN*) generated within the ASR, plus inflow (*INF*) from any upstream ASR that flows directly into it, as described by Strzepek *et al.* (2013):

$$WSI = \frac{TW}{RUN+INF}$$

For only the municipal and industrial sectors, water requirements included in *TW* are represented by consumptive use in the model—with additional consideration for reuse within the basin to assess total withdrawal[3]. To estimate withdrawal, we use common ratios that represent the fraction of consumption over withdrawal. Inflow to any given ASR is a consequence of flow regulated from upstream ASRs; therefore WSI is an evaluation metric of the managed water system as simulated by WRS. Irrigation receives its total withdrawal, with its return flow credited to the downstream ASR (see Strzepek *et al.*, 2013 for details). We characterize the severity of water stress according to Smakhtin (2005), which classifies an ASR's water use as slightly exploited when WSI < 0.3; moderately exploited when 0.3 ≤ WSI ≤ 0.6; heavily exploited when 0.6 ≤ WSI ≤ 1; overly exploited when 1 ≤ WSI < 2; and extremely exploited when WSI ≥ 2. Similar water-stress indices are computed in other studies and generally consider a threshold of 0.4 to indicate severe water limitation (e.g., Vörösmarty *et al.*, 2000; Wada *et al.*, 2011). **Figure 6** shows the WSI for the baseline scenario. As shown, a large portion of northern China as well as India and the Indus River systems experience at least moderate to extremely exploited water conditions.

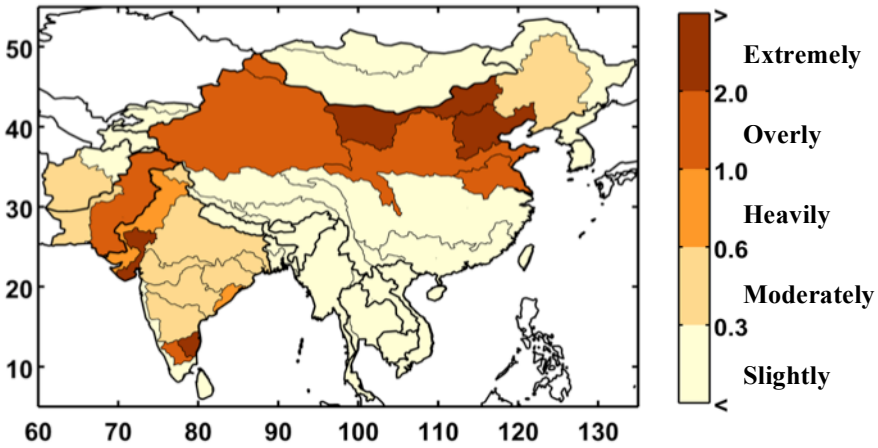

Figure 6. Distribution of water stress index by ASR, as simulated by IGSM-WRS from the baseline climate run.

[3] Based on the assumption that any return flow (withdrawal in excess of consumption) is likely returned to the ASR's storage within the month. This assumption is not appropriate for irrigation because return flow, which may be substantial, may not be returned to the ASR storage immediately.

3. RESULTS

3.1 Distributional Changes in Climate Parameters

In the IGSM-WRS framework, two variables respond to changes in climate: runoff, which provides surface water supply to the ASR; and irrigation requirement, which is an estimation of farming water requirements. The baseline runoff is shown in **Figure 7** in billion cubic meters (BCM). In general, there is substantial runoff in the southeast, which benefits from a wet and humid climate, while the north and far west of the region are especially dry. Note that, in order to keep units consistent, runoff is not normalized by area, so larger ASRs have more runoff in part due to the contributing land area.

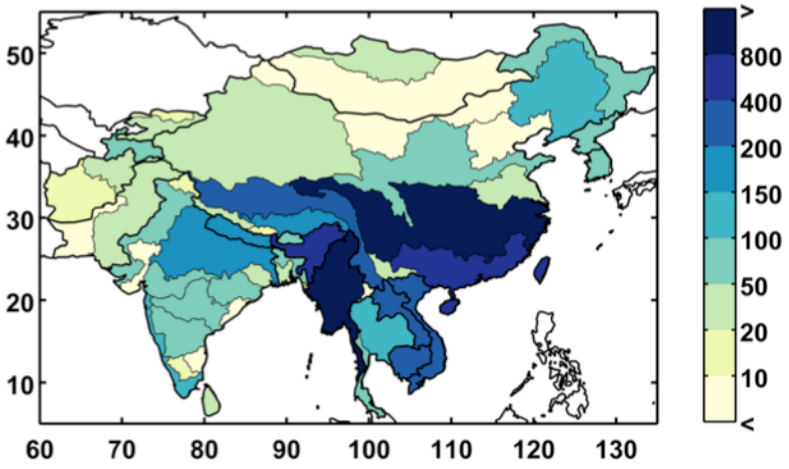

Figure 7. Baseline annual runoff by ASR (in billion cubic meters per year).

We take two approaches to present the large number of future runoff changes: (1) we show example maps of probability points on the distribution of a single metric, maintaining the geographic spatio-temporal patterns in each scenario, and (2) we simplify complex results by ignoring spatio-temporal correlations and mapping points for specific values in the ASR probability distributions. For (1), first we characterize the resulting runoff of each scenario using a single metric across area and time. We find a strong likelihood that runoff will increase for the majority of the population (**Figure 8**). The values shown (as a cumulative probability distribution) are calculated using a population-weighted mean of the percent change in annual runoff from all the ASRs by 2050, with ensemble members sorted from driest to wettest. Around 90% of scenarios suggest an overall increase in runoff. While the scenarios shown in **Figure 8** indicate a predominate tendency toward a relative increase in runoff *averaged for the entire region*, we find that the variability across ASRs is quite diverse.

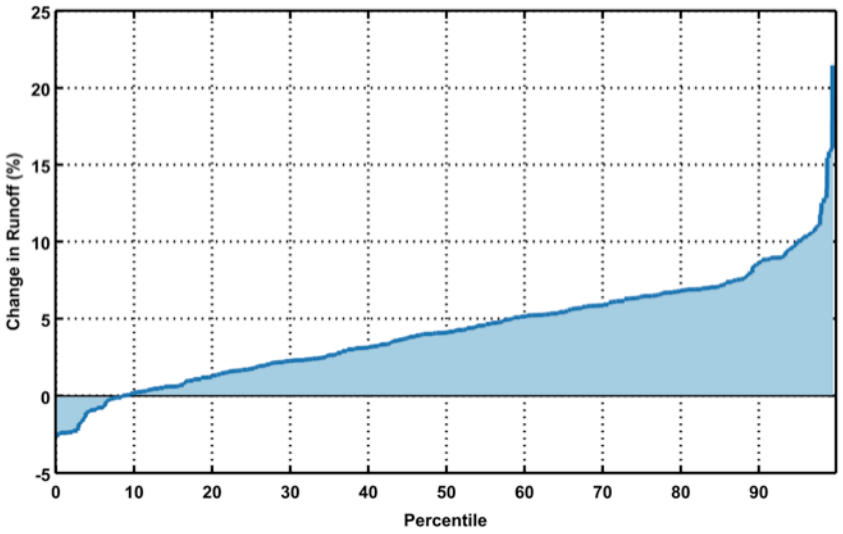

Figure 8. Percentage change in runoff across all ensemble members. Each point in the line represents one of the 551 members with appropriate weights from the Gaussian Quadrature (Section 2.3). The percent change in runoff represents a weighted-averaged result for the entire domain of study region (Fig. 1) - such that for every member's result in the distribution shown, each ASR's runoff has been weighted by its population (Fig. 3).

Figure 9 highlights this situation. The first column shows results around the 10th percentile, the second column around the median, and the third column around the 90th percentile. With these we can see there are patterns that persist in most cases, e.g., a wetter result in southern central India and much of Southeast Asia, or drier result in western Pakistan and Afghanistan, but many of the ASRs provide varying results depending on the specific climate pattern. The diversity in the regional patterns of runoff change is further illustrated by mapping the 10th, median, and 90th percentiles of runoff change for each ASR in a "point-wise" fashion (**Figure 10**). As a result, these maps display a general inference about the runoff change distribution at each ASR, but do not represent the likelihood of a specific climate pattern. In this context, for any given ASR, a wetter climate would be anticipated for those in the southern portions and a drier climate in the north, as compared to the baseline scenario. Southern India and the Indo-Chinese peninsula are especially prone to a wetter future climate as reflected by increased runoff in 90% of the scenarios; Afghanistan, Pakistan and portions of China are especially prone to a drier future climate, as 90% of the scenarios indicate decreased runoff.

The other calculated metric within the WRS framework that is influenced by the IGSM's climate response and pattern-scaling is the irrigation requirement—an estimate of the amount of water that farming in an ASR would use if there were an abundant water supply (given irrigated area per crop and irrigation efficiencies). In this modeling framework, irrigation requirement responds to changes in precipitation and temperature, rising when soil conditions are drier and falling when they are wetter, without exceeding the maximum water needed by the crop. Baseline irrigation requirement is shown in **Figure 11**. We calculate the percentage change in irrigation requirement, weighted by population, for each scenario. A distributional summary across the ensemble members is shown in **Figure 12**, ordered from least to greatest. A majority of the simulations result in increased irrigation requirement, i.e., a drier climate, in about 70% of

the scenarios. This result seems to be in conflict with runoff changes, which is responding to the same climate as the irrigation requirement. The reason for this conflict lies in the complexities of the two mechanisms—climate conditions are not simply wet or dry. For example, the irrigation requirement is highly dependent on the growing season and irrigated area of each crop. In some cases, the results show changes in seasonal climate patterns, with a drier growing season and wetter dormant season, resulting in a wetter climate overall. Another reason for the conflict is that excess water for irrigation is ignored in the irrigation requirement estimation; we only estimate the amount of water the crops require, which is not satisfied by rainfall, to obtain a yield without water stress. In the case that a crop receives all it needs from rainfall in the baseline scenario, an increase in rainfall does not change the irrigation requirement.

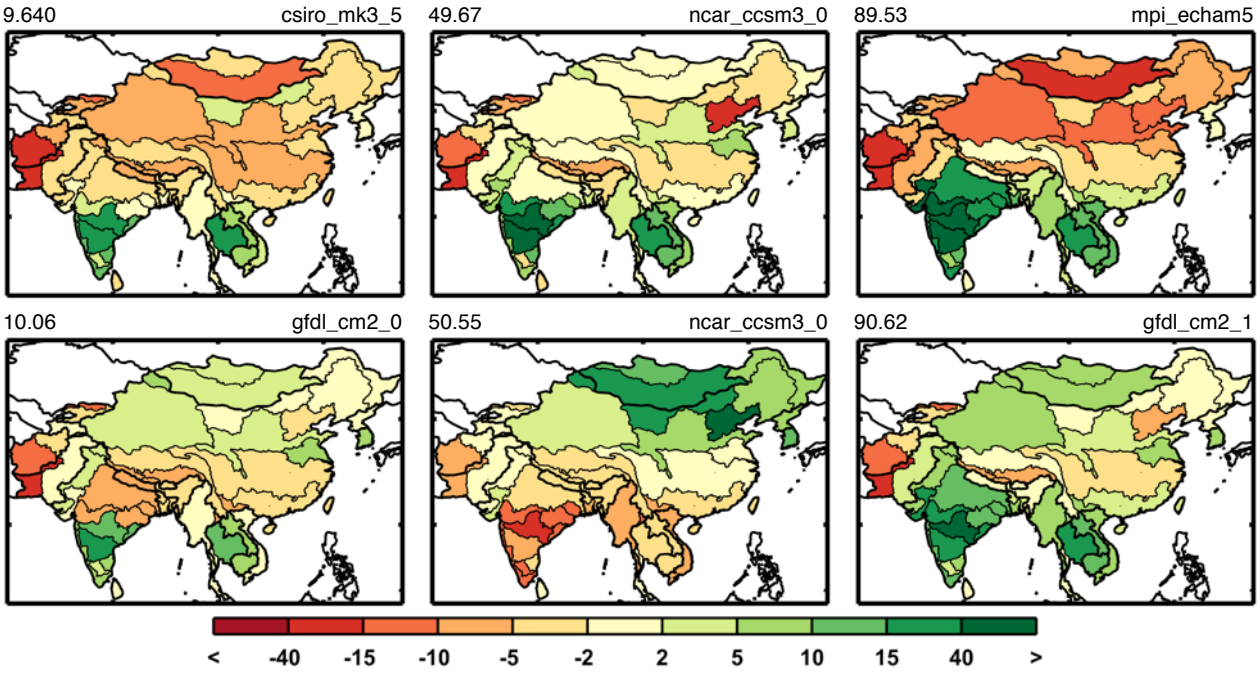

Figure 9. Runoff change patterns (in %) around the 10th, 50th, and 90th percentile, two each based on the mean runoff change for the region (the metric used in **Figure 8**). Top label shows the percentile (left) and the GCM name (right.)

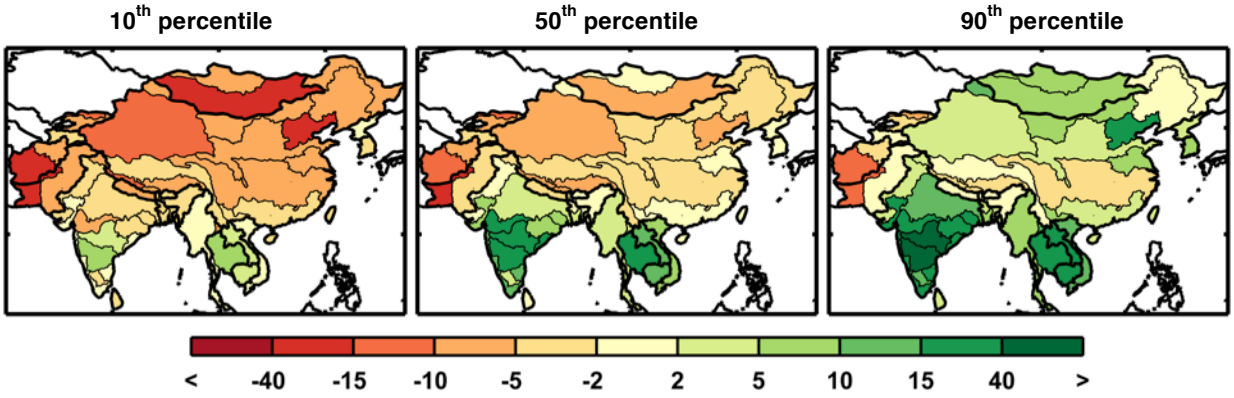

Figure 10. Changes in ASR runoff (%) calculated point-wise by ASR, showing changes in decadal averaged ASR runoff from the baseline to the future scenarios averaged over 2041–2050 for the 10th, 50th, and 90th percentiles.

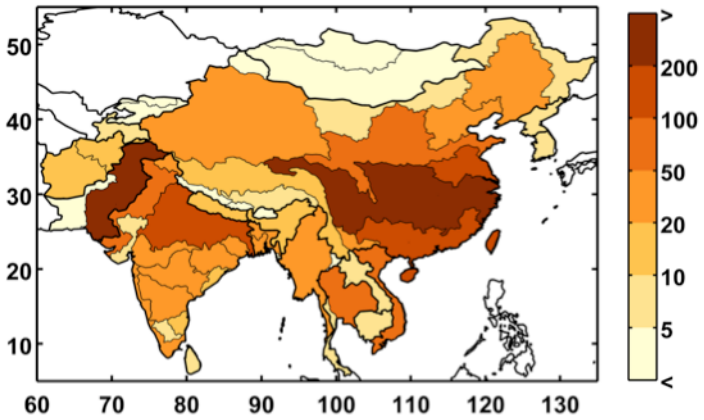

Figure 11. Baseline irrigation requirement (in billion cubic meters)

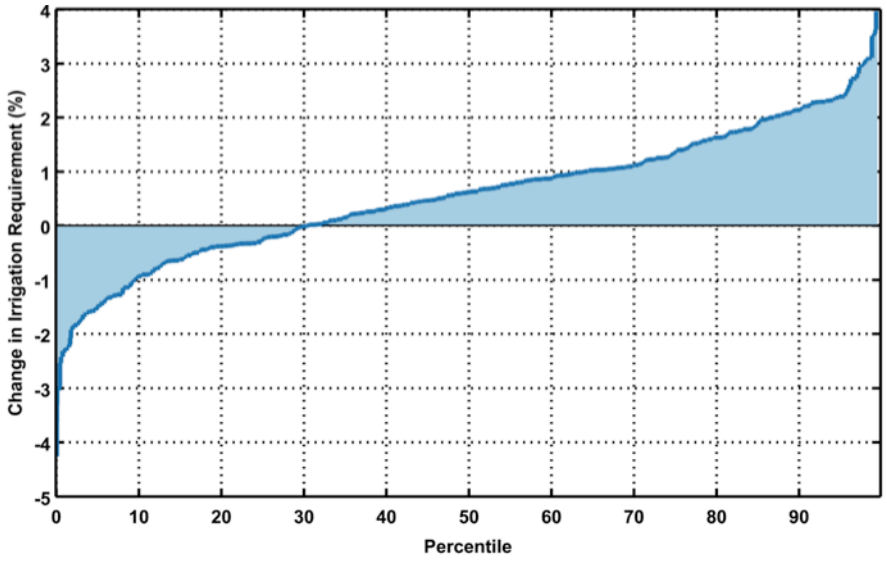

Figure 12. As in Figure 9, but shown for percentage change in irrigation requirement across all ensemble members. Each point in the line represents one of 551 climate scenarios.

Similar to **Figure 9**, in **Figure 13** we show examples of six maps of changes in irrigation requirement: two from ensemble members near the 10th percentile, two near the 50th percentile, and two near the 90th percentile results. Again, we see that different climate patterns can result in a similar value of the metric used in **Figure 12**. In these examples, we do see a general wetting in the south and southeast and drying in the north and west, although not all examples shown adhere to these general patterns.

Similar to the point-wise maps of runoff shown in **Figure 10**, individual ASR changes in irrigation requirement are mapped in **Figure 14**. Since precipitation and temperature are the main drivers for both runoff and irrigation requirement estimations, we see a similar pattern in both maps, with the north drier (i.e., increased irrigation requirement) and the south wetter (i.e., decreased irrigation requirement). Since the irrigation sector is by far the largest requirement for water in this region, small changes in mean irrigation requirement can have a substantial impact on the water sector within each ASR.

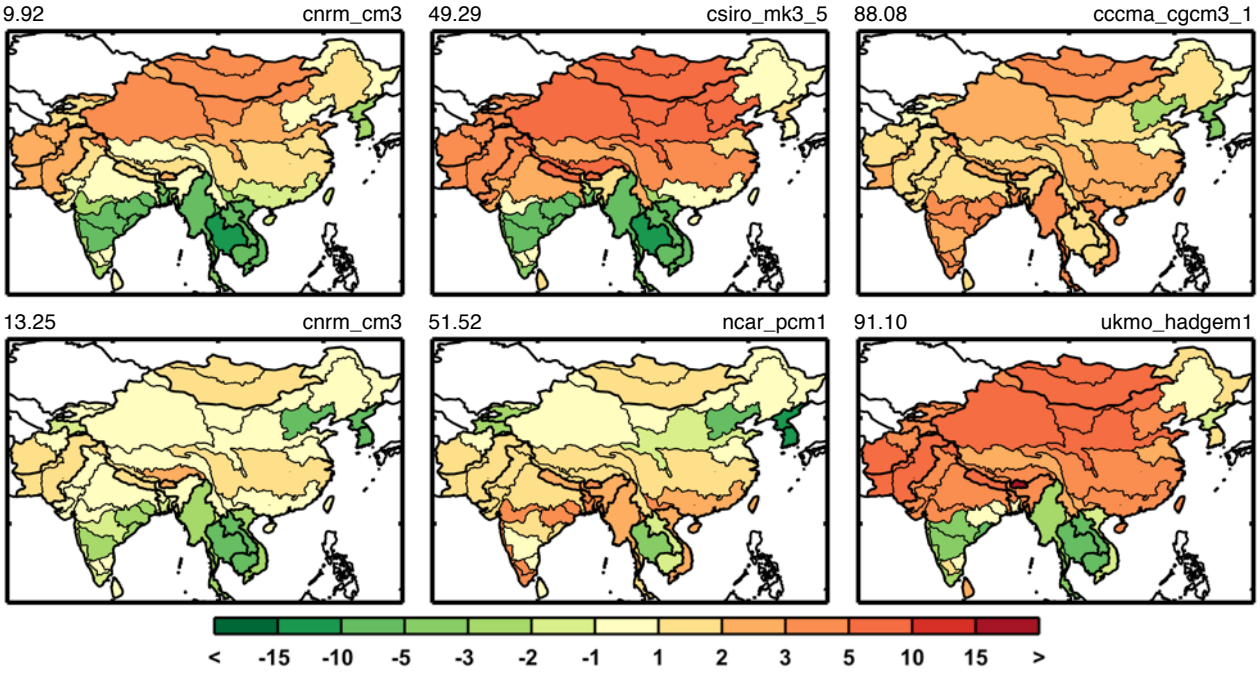

Figure 13. Irrigation requirement change patterns (in %) around the 10th, 50th, and 90th percentile, two each based on the mean irrigation requirement change for the region. Top label shows the percentile (left) and GCM name (right.)

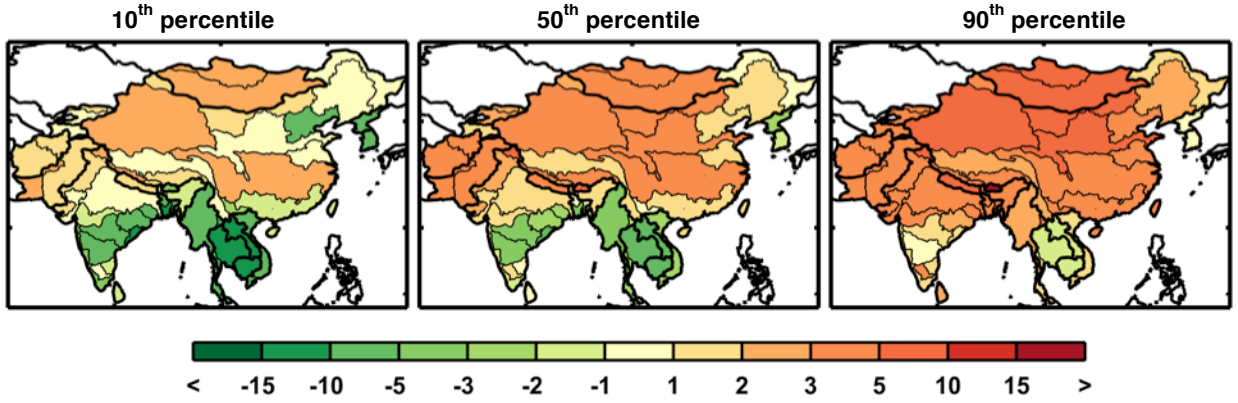

Figure 14. Changes from baseline in irrigation requirement (%) calculated point-wise by ASR, showing changes in decadal averaged ASR irrigation requirement from the baseline to the future scenarios averaged over 2041–2050 for the 10th, 50th, and 90th percentiles.

3.3 Distributional Changes in Growth Parameters

Domestic and industrial water requirements are both driven by changes in growth in the WRS framework. Although these consumptive requirements are smaller than the irrigation requirements in the baseline scenario, in most ASRs they do play a significant role in the future scenarios, depending on population growth and GDP projections.

3.3.1 Domestic Water Requirements

Domestic water requirement for the baseline scenario is shown in **Figure 15**. Taking a similar approach as with the runoff and irrigation requirements, a region-wide estimate of domestic water requirement is shown in **Figure 16** as a percent change, weighting each ASR value by population. Compared to changes in irrigation requirement, domestic water requirement grows substantially percentage-wise, with an 80% to 180% increase. But, since the baseline domestic requirement is small compared to the baseline irrigation requirement (see Figs. 11 and 16), the total amount of increase in requirement is relatively small.

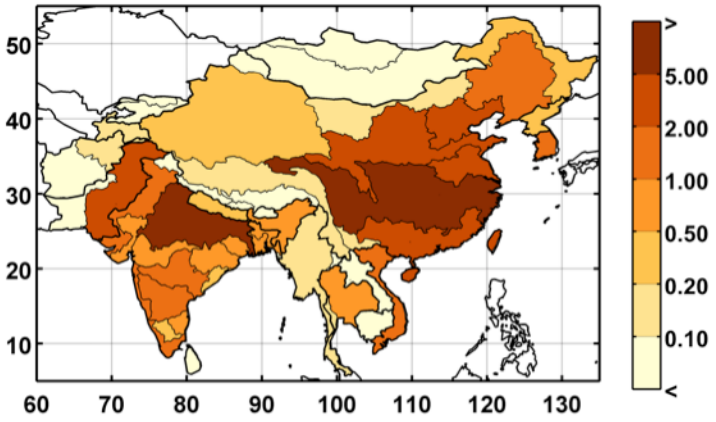

Figure 15. Baseline domestic water requirement (in billion cubic meters).

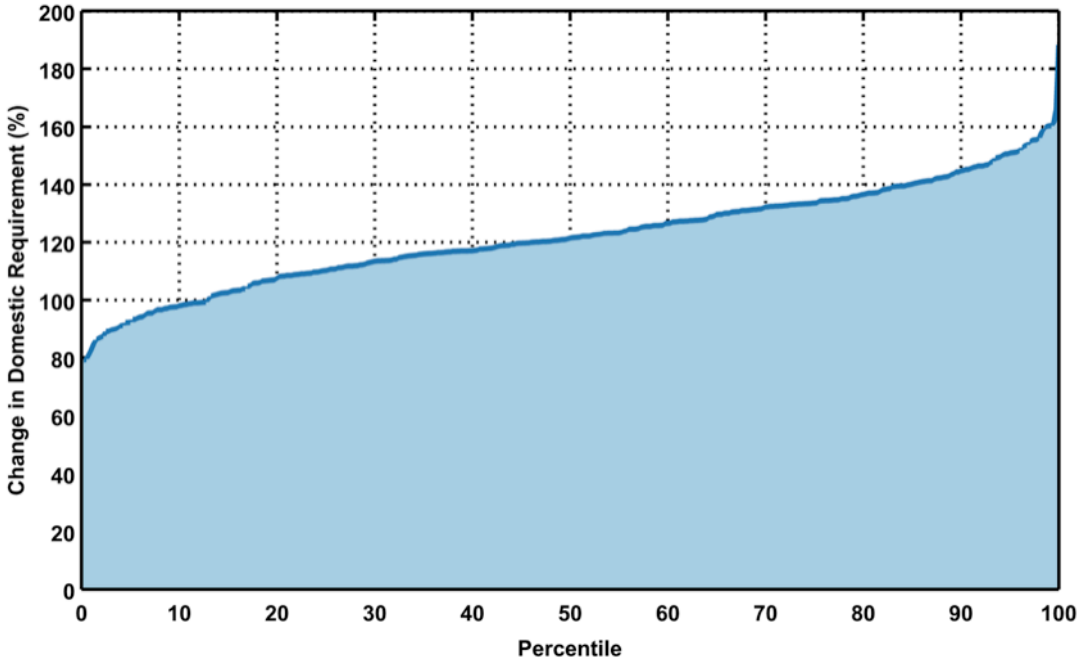

Figure 16. As in Fig. 13, but for percent change in domestic requirement for the region for all scenarios. Each point in the line represents one of 400 growth scenarios. Percent change for each ASR in each scenario is weighted by population.

Now we analyze the variety of domestic water requirement mapped across the region (shown in **Figure 17**). For the growth parameters, the variety of changes across the region is derived from the EPPA results and is important in order to be consistent in terms of the interaction of the region's socio-economics by EPPA region (Figure 1).

Figure 18 summarizes the distributional changes in domestic water requirement (2000–2050) across scenarios by presenting the 10th, 50th and 90th percentiles, calculated individually for every ASR. Contrary to irrigation requirement, this water demand *only increases* across all the ASRs for the future. China is expected to see relatively small increases in domestic requirement compared to Mainland Southeast Asia and parts of India, where substantial increases are expected—between 2 and 5 times the baseline values.

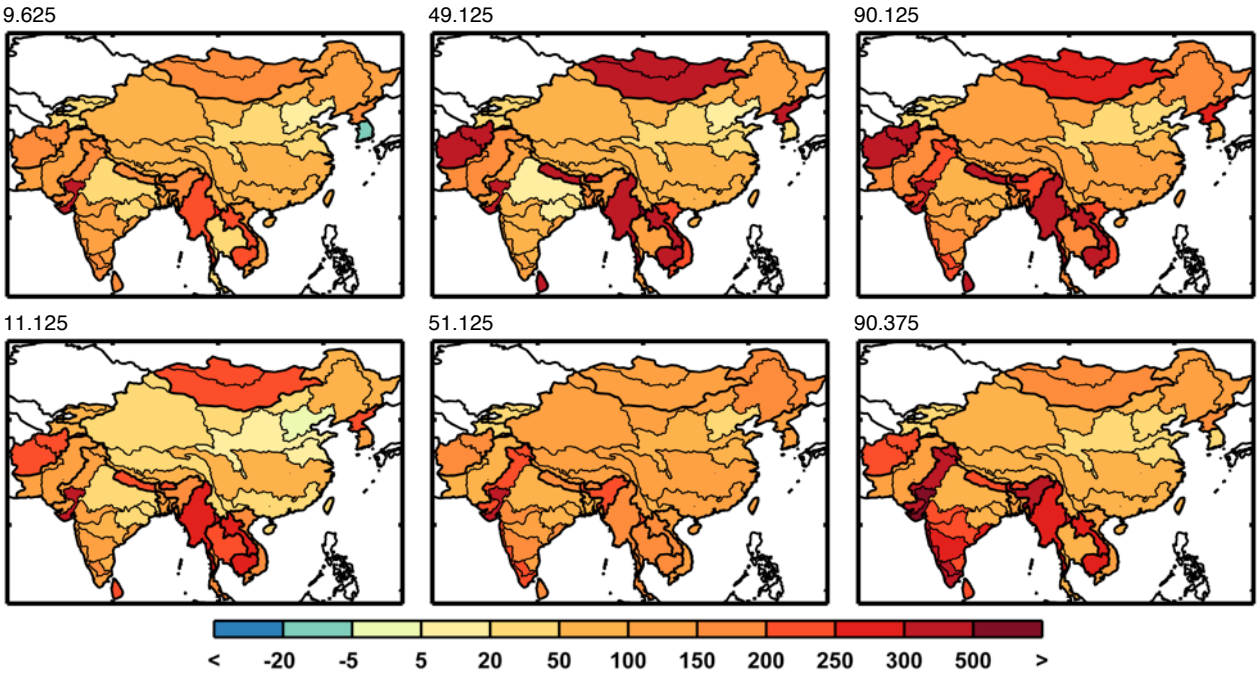

Figure 17. Domestic water requirement change by region (in %) around the 10th percentile, median, and 90th percentile, two each, similar to the metric used in **Figure 16**. Top label shows the percentile.

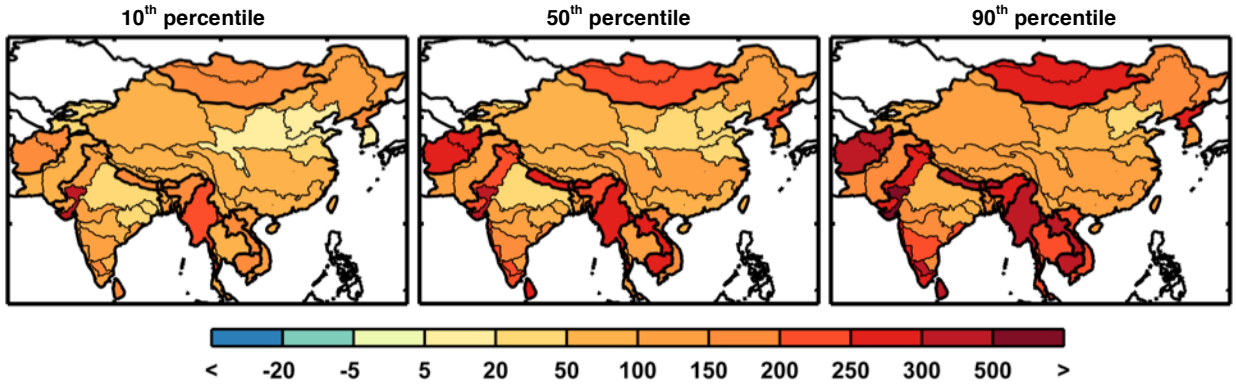

Figure 18. Changes from baseline in domestic water requirement (%) calculated point-wise by ASR, changes are based on the baseline (Fig. 16) to the future scenarios averaged over 2041–2050 and shown for the 10th, 50th, and 90th percentiles for each ASR.

3.3.2 Industrial Water Requirement

In this model framework, the industrial water requirement responds to changes in per capita GDP. The baseline industrial water requirement is shown in **Figure 19**. A large portion of the industrial requirement is in China, with a fair amount in India and Vietnam.

Figure 20 shows the inverse cumulative distribution of population-weighted percent change in industrial requirement. Industrial requirement varies considerably across scenarios, ranging from 60% increase to 440% increase from baseline, with a median of about 200%. In **Figure 21**, six examples of the variety of industrial water requirement changes are shown across scenarios of similar percentiles based on the mean percent change weighted by future population. Here we can see the richness of the scenario members' patterns derived by the socio-economic modeling.

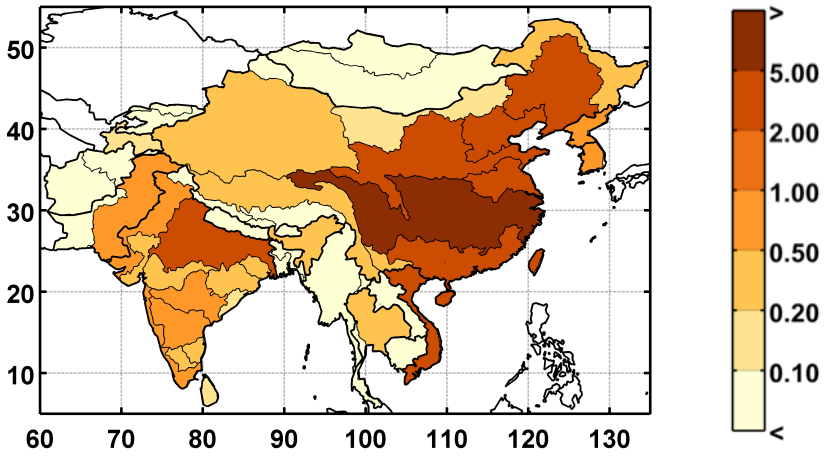

Figure 19. Baseline industrial water requirement (in billion cubic meters).

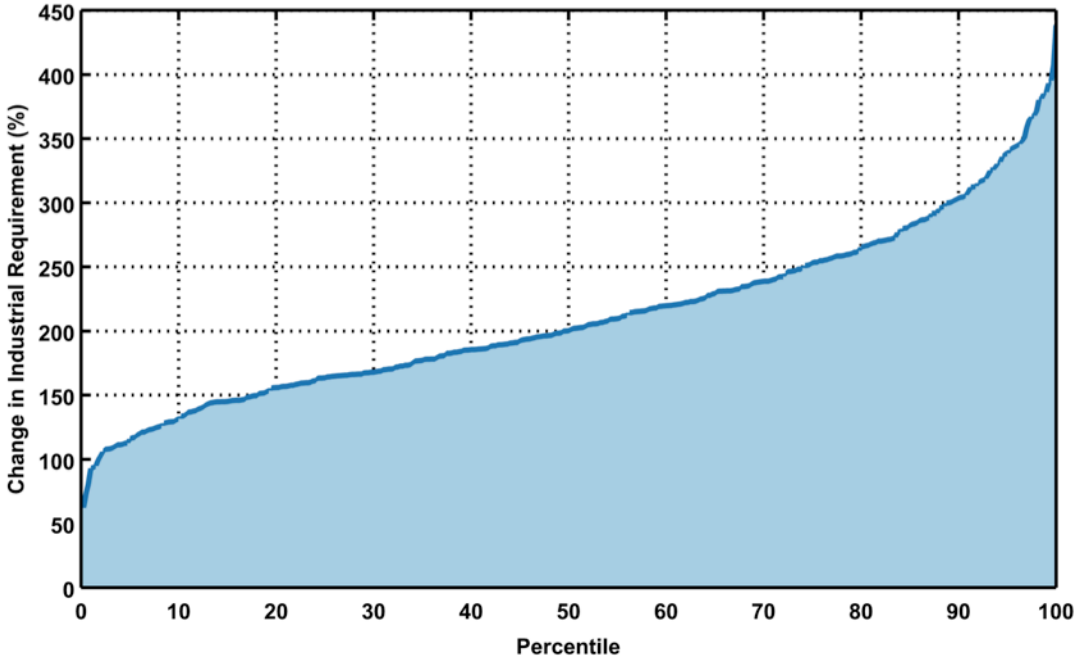

Figure 20. Mean change in industrial requirement for the region for all scenarios. Each point in the line represents one of 400 growth scenarios. Percent change for each ASR in each scenario is weighted by population.

Once again, using the probability distribution of each individual ASR, we calculate and map the 10th, median, and 90th percentiles, shown in **Figure 22**. Here we see that the industrial requirement for ASRs in India and China increase considerably, by about two or three times the baseline amount in the median case and three to four times in the 90th percentile.

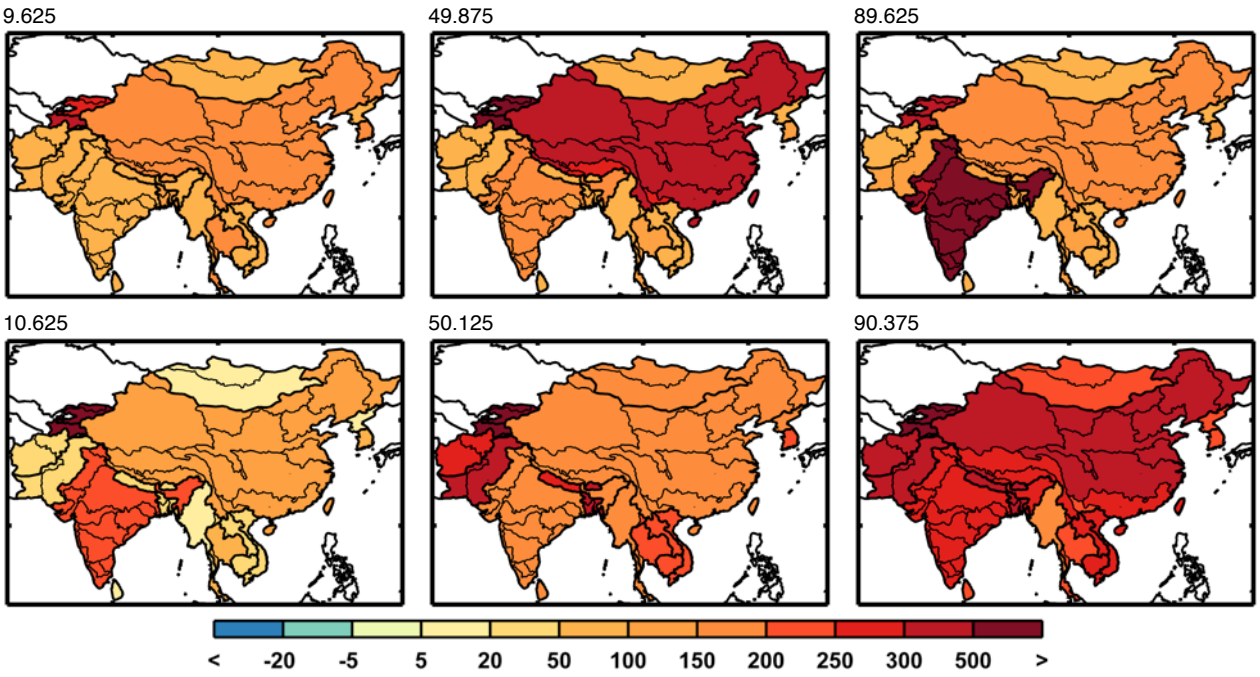

Figure 21. Industrial requirement change (in %) around the 10th percentile, median, and 90th percentile, two each, based on the mean industrial requirement change for the region (the metric used in **Figure 20**). Top label shows the percentile.

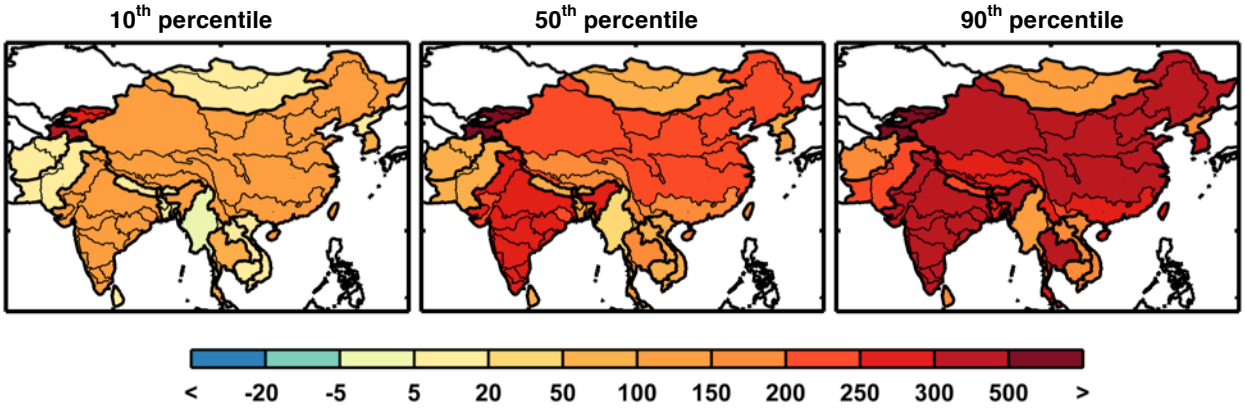

Figure 22. As in Fig. 19, but for industrial water requirement shown for the 10th, median, and 90th percentiles for each ASR.

3.4 Mapped Changes in Water Stress

As previously discussed (Section 2.4), we assess changes in water stress via two measures: UWR and WSI. We will also evaluate these changes across three ensembles: *Just Growth*, *Just*

Climate, and *Climate and Growth*. For the *Just Growth* ensemble, we run the model with the baseline climate, changing only the growth parameters—population and GDP—which affect domestic and industrial water requirements. With this ensemble, we isolate the effects of growth by removing the effects of climate. In the *Just Climate* ensemble, we keep the growth parameters constant at the year-2000 value, and provide the model with a different future climate projection for each scenario. With this ensemble, we remove the effect of growth and focus on the effect of climate change. In reality, growth and climate occur simultaneously; however, for policy decisions, distinguishing growth effects from climate change effects is important since policy rarely targets both growth (e.g., population or wealth) and climate (GHG mitigation) simultaneously. We are also interested to assess the degree to which the effects of growth and climate interact non-linearly. Hence, we run a final ensemble, *Climate and Growth*, which combines the two effects, and represents the future we face under an "unconstrained emissions" pathway.

In **Figure 23** the 10th, 50th, and 90th percentiles of UWR point-wise distribution are mapped for each of the three scenario groups. For the *Just Growth* scenario group, we see UWR increasing or remaining constant, even in the 10th percentile, although there are some basins that are affected by growth changes more than others. In the *Just Climate* scenario group, driven by the changes in runoff and irrigation requirement, UWR decreases in the south, for much of India and the

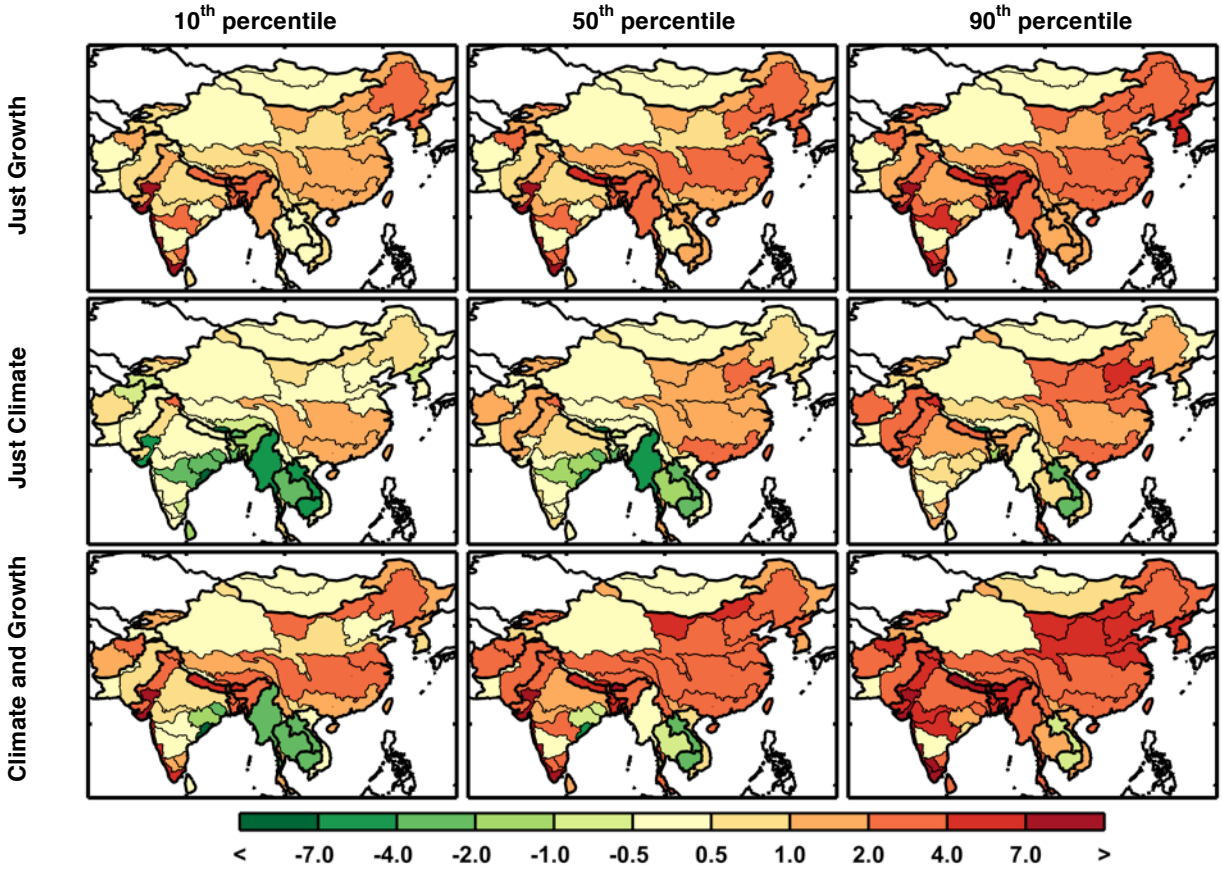

Figure 23. Exceedance changes in ASR UWR (%). Changes are based on the baseline (Fig. 6) to the future scenarios averaged over 2041–2050 and shown for the 10th, 50th, and 90th percentiles for each ASR.

Indo-Chinese Peninsula, and increases for much of China (especially in the east), Afghanistan and Pakistan. For the *Climate and Growth* median case, we find many similarities to the *Just Growth* scenario. UWR increases in almost all of the ASRs, with exceptions in Cambodia, Laos, Thailand, and eastern India; this suggests that the positive climate effects outweigh the negative growth effects in the south while the negative climate and growth effects are compounding in much of China. Appendix A shows the distribution of scenarios using the population-weighted change in UWR and the example maps around specific points in the distribution using that single metric.

Figure 24 shows series of maps for the WSI similar to that shown for UWR in Figure 24. Results for the three ensembles are mapped for every ASR based on specified exceedances—10th, 50th, and 90th percentiles. There is a similar overall pattern to this stress index as was shown for UWR. Stress increases in all maps as a response to the growth changes, while there are some positive and negative responses to changes in climate. However, when we combine these two effects in the third row of maps, the majority of the benefits are overpowered by the negative effect of growth, with the exception of two ASRs in southern India in the median map. For the 90th percentile results, all ASRs show increased WSI.

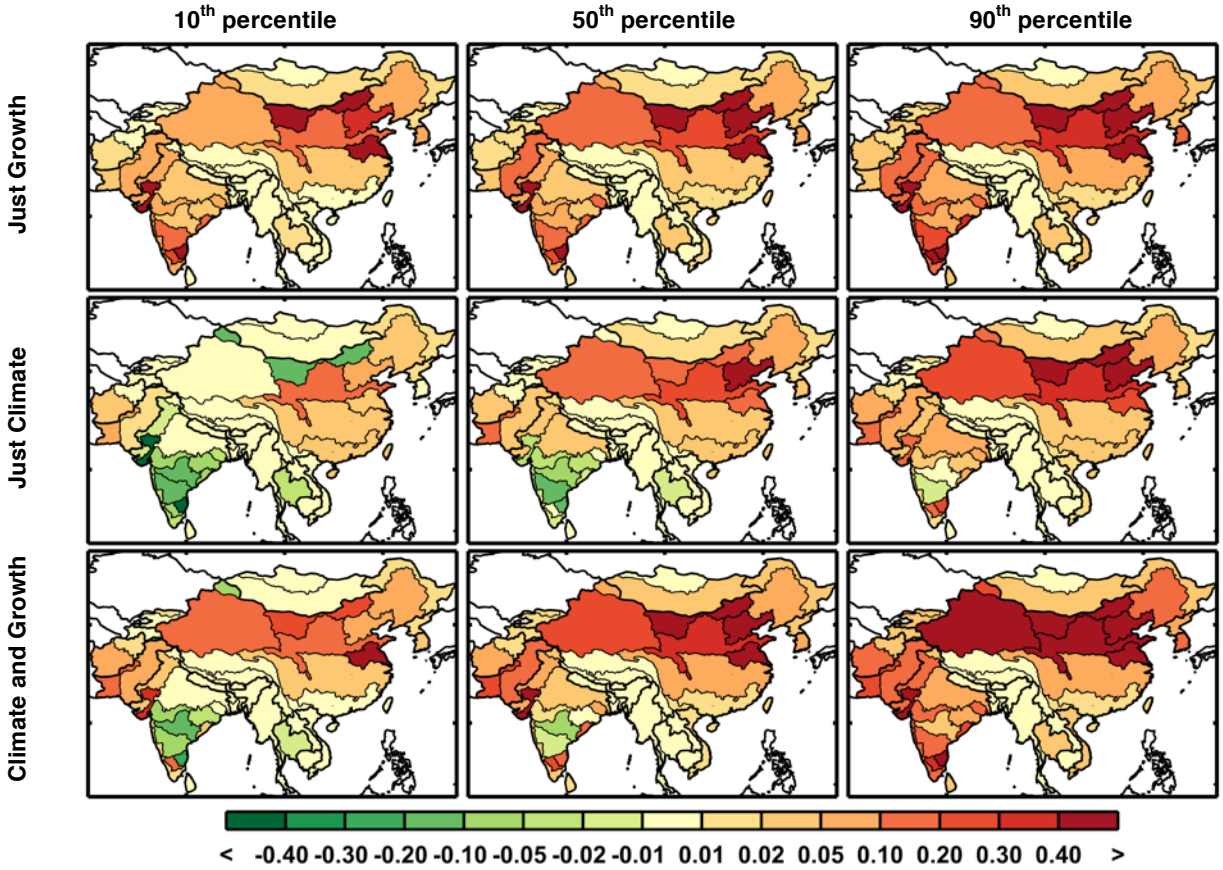

Figure 24. Exceedance changes in decadal averaged WSI (unitless). Changes are based on the baseline (Fig. 7) to the future scenarios averaged over 2041–2050 and shown for the 10th, 50th, and 90th percentiles for each ASR.

Another way to show the distributions of each ASR is to map the exceedance probability of specific WSI values. **Figure 25** shows the exceedance probabilities at three distinct levels of WSI: probability of a future WSI higher than the baseline, probability of increasing at least 0.05, and probability of increasing at least 0.2. In many of the basins we consider, we find that these exceedance values (0, 0.05, and 0.2) were derived from the historical bootstrap presented in the next section, where a change of 0.05 is larger than the variance of the bootstrapped history and a change of 0.2 is larger than the range of the bootstrapped history. For the *Just Growth* ensemble, the probability of increasing WSI is 100% for all ASRs, but most of the ASRs (especially Southeast Asia) have a lower probability of a substantial WSI increase (i.e., greater than 0.05). In northern China and southern India, there is a much larger probability of a substantial WSI increase. For the *Just Climate* ensemble, the southern portion of the region has a low probability of increasing WSI, while the northern portion, including China, has high probability; although, in southern China, the increase in WSI is likely to be less than in northern China. The *Climate and Growth* ensemble results in larger stress probabilities across the three WSI increase thresholds that are, again, higher in the south than the north and west of the region.

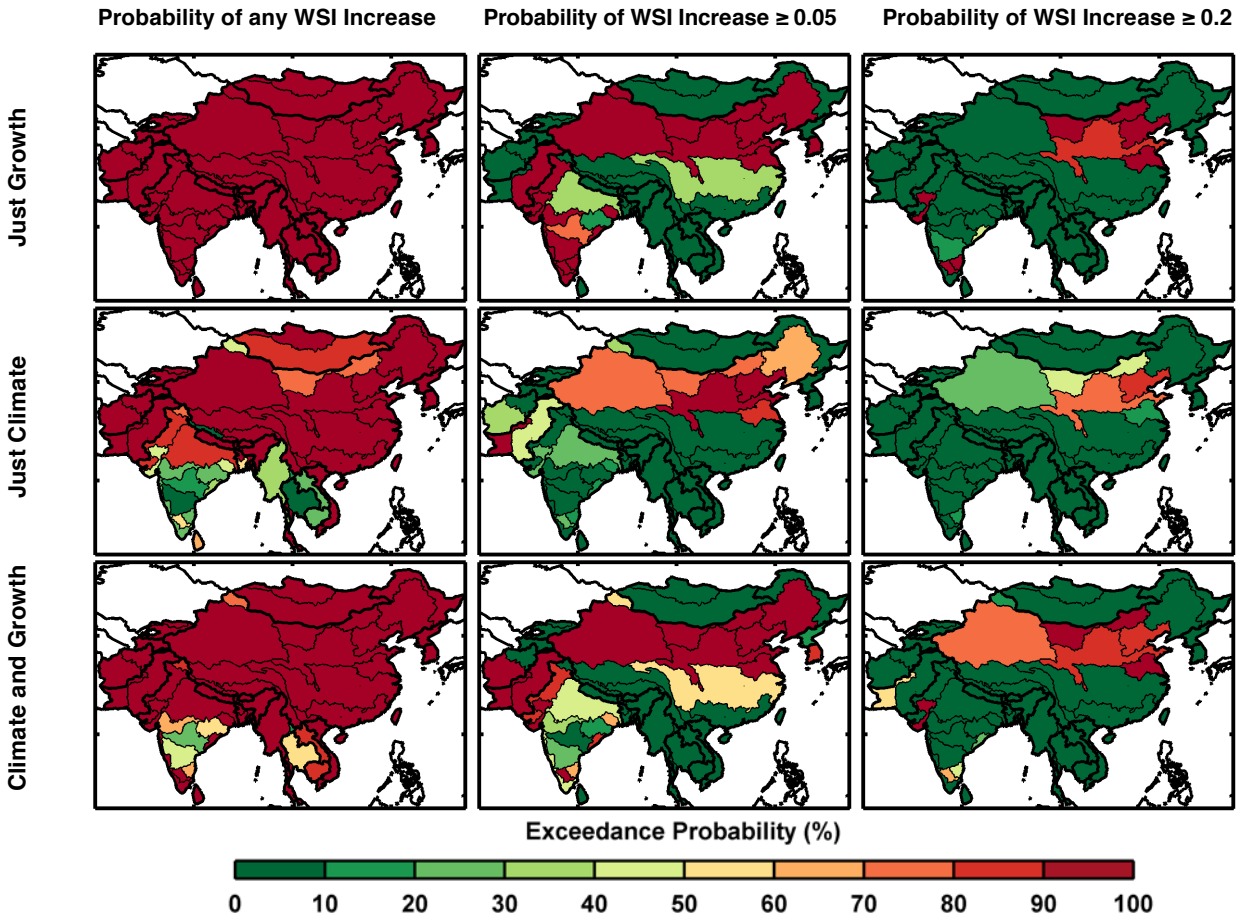

Figure 25. Probability of exceedance for change in WSI. Changes are based on the baseline (Fig. 7) to the future scenarios averaged over 2041–2050. Columns are % probability of WSI increase: > 0 (left); > 0.05 (center); and > 0.2 (right). Scenarios: Just Growth (top row), Just Climate (middle row), and Climate and Growth (bottom row).

We apply the same mapping technique to UWR (**Figure 26**), with three increase thresholds: probability of increasing, probability of increasing at least 2% and probability of increasing at least 4%. Again, these values are deemed significant based on the historical bootstrap shown in the following section. For *Just Growth*, with few exceptions most ASRs increase UWR in all scenarios; most will likely increase between 0 and 4%. For *Just Climate*, southeast Asia is generally less likely to increase UWR, but most ASRs in China and India are likely to experience increases between 0 and 2%. In the *Climate and Growth* ensemble, most of southeast Asia and India show increases in UWR between 0 and 2%, although some show low probability of increasing at all. For the majority of China, the increases in UWR are more likely to be between 2% and 4%.

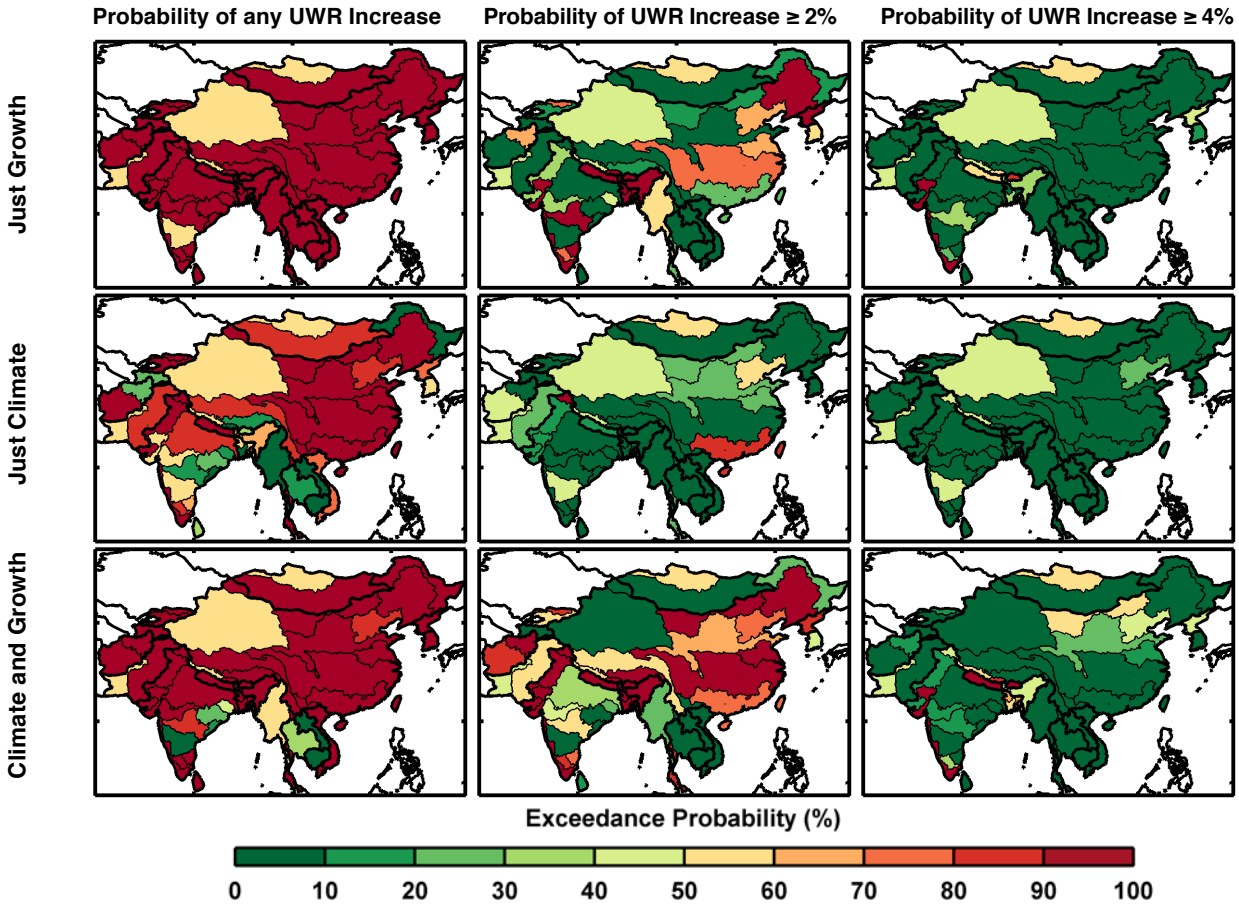

Figure 26. As in Figure 26 but for probability of exceedance for changes in UWR. Columns are % probability of UWR increase: > 0 (left); > 2 (center); and > 4 (right). Scenarios: Just Growth (top row), Just Climate (middle row), and Climate and Growth (bottom row).

3.5 Water Stress Frequency Distributions

Next, we show the frequency distributions of outcomes to qualify the consequences of the scenarios in terms of future risk. We select specific regions, first by political boundaries and second by hydrologic basin boundaries (see **Figure 28**), and calculate the aggregate water stress for 2041–2050 over the region, with ASR values weighted by population. As in the previous section, we compare these WSI changes with the baseline scenario WSI. Recognizing that the baseline scenario is only one of many possible traces of climate through time, we develop a *baseline ensemble* to understand the range of water stress that results from the impact of climate sequences on water availability. To do this, we use a multivariate k-nearest-neighbor bootstrap approach (as discussed in Lall and Sharma, 1996) to develop this baseline ensemble of 500 members, each containing a 50-year time series of the required WSM climate-dependent input data including monthly values of irrigation requirement, runoff, and reservoir evaporation. Lall and Sharma (1996) shows that the multivariate k-nearest-neighbor bootstrap approach has the advantage over simple bootstrapping in that it maintains the lag-1 correlation as well as geospatial correlations. As constructed, the baseline ensemble can be viewed as a statistically based emulation of the uncertainty in the WRS projection caused by the natural variability of climate – which is inherently unpredictable

In **Figure 28**, we show the two stress indices using a kernel smoothing approach to approximate the shape of the distribution of three major political regions (as shown in **Figure 27**): China, India, and Mainland Southeast Asia. These plots show characteristics of the distributions, e.g., mode, skewness and the nature of the distribution tails. The three future ensembles—*Just Growth* in red, *Just Climate* in blue, and *Climate and Growth* in yellow—are shown as the difference from the last decade of the baseline scenario value (2040–2050) and that of the future result. The baseline ensemble distribution (in grey) shows the difference between the 50-year baseline scenario mean and the last ten years of each baseline ensemble member. The baseline scenario-mean value is also printed above each plot. We can thus compare the distributions from natural variability (the grey distribution) to the range of the future water stress ensembles to understand the magnitude of the uncertainty derived from changes in climate, growth, or both.[4] In China, both growth and climate have adverse effects but growth is slightly stronger. The *Climate and Growth* ensemble is, as expected, worse but not simply an aggregate of the two. In India, climate has either a slightly positive effect, as is shown in the WSI distribution, or no effect where the mode is around zero change. Growth has a strong negative effect, and the combined ensemble is dominated by this effect. We see this to be especially true in the UWR distribution. In Mainland Southeast Asia, climate is mostly beneficial to the water supply but growth is not, resulting in a combined effect that is close to no change. Note that the natural variability distributions are rarely wider than the distribution of the future ensembles, but in some cases (e.g., WSI in Mainland Southeast Asia) future uncertainty by the 2040s is close to the historical uncertainty.

[4] We remove the natural variability from the changes in these future WSIs by comparing them with the baseline, which contains the same natural variability. This is an effect of using the delta method, and allows us to focus on long-term mean changes, isolating the effect of the climate change trend from that of natural variability in climate.

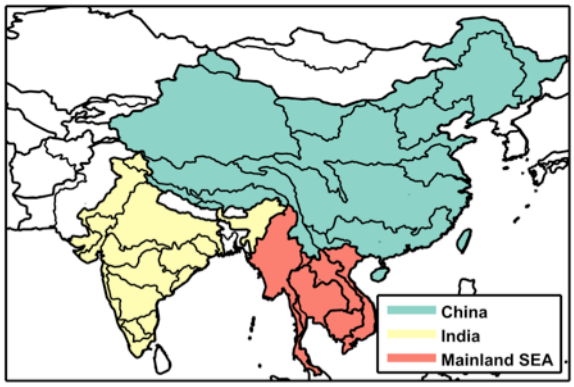

Figure 27. Map of major political regions showing the aggregate frequency distributions of water stress.

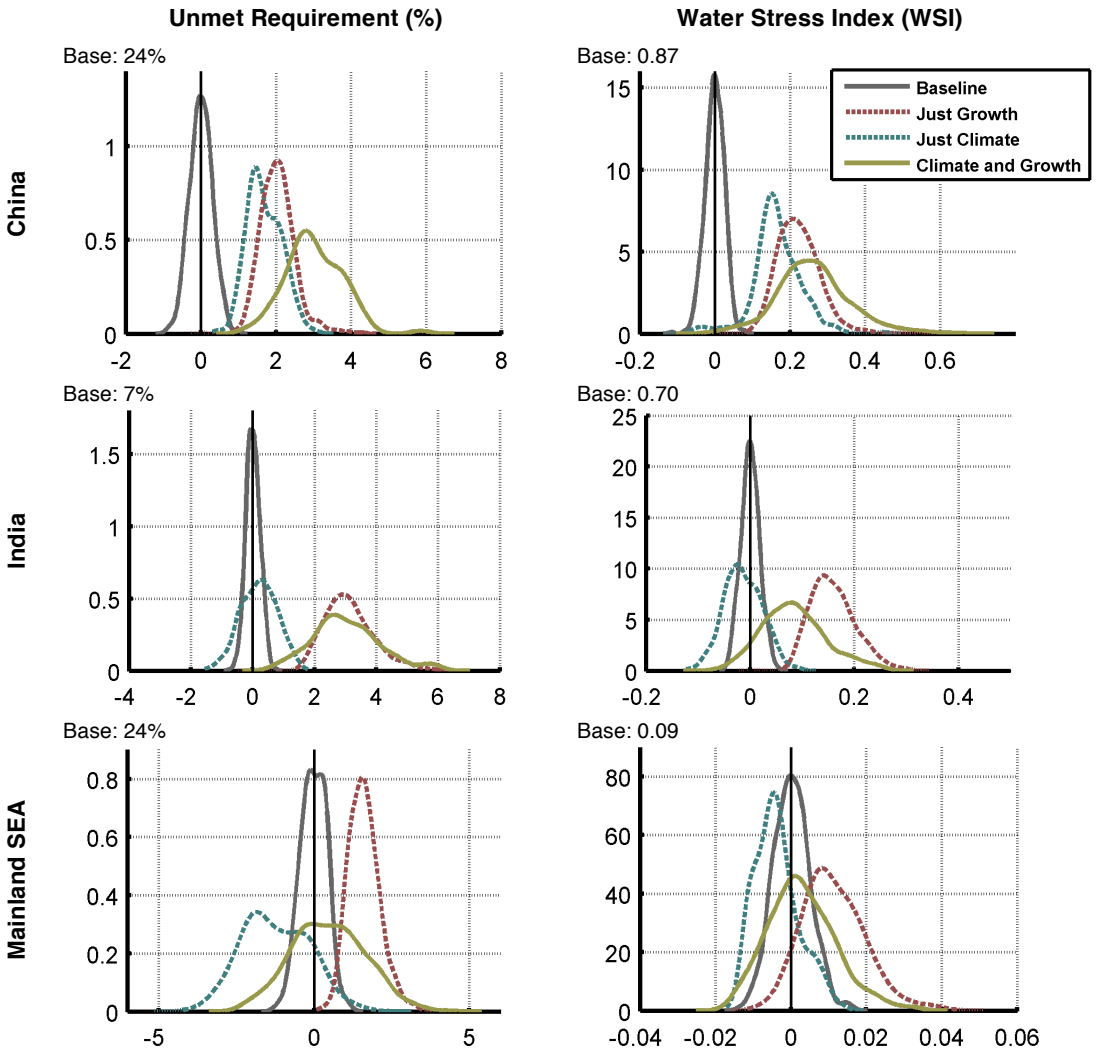

Figure 28. Frequency distributions of changes in decadal averaged Unmet Water Requirement (UWR, left) and water stress index (WSI, right) for 2041–2050 against the baseline result aggregated over major socio-economic regions (Fig. 28) and weighted by population. Mean baseline value shown above each figure. Results are shown for the Just Growth, Just Climate, and Climate and Growth ensemble scenarios. In addition, a distribution for the Baseline result is also provided that depicts the range of UWR and WSI decadal-averaged changes that would result from internal variability of the climate forcing (see text for details).

Next, we aggregate by basin (see **Figure 30**), again using population to give each ASR a respective weight. These basins were chosen because their rivers cross country boundaries and could be a cause for political tension. As seen in **Figure 31**, in the Indus Basin, shared mostly by India and Pakistan, there is considerable stress in the baseline case; climate and growth both increase stress further, and few scenarios result in a stress decrease. In the Ganges basin, climate and growth both increase stress for most of the scenarios; climate is less potent than growth in terms of UWR, but has a similar effect in the WSI. The Mekong and Brahmaputra basins both reside in wet climates with low storage basin-wide. These areas are also major producers of paddy rice, a water intensive crop, which results in high UWR. In the Mekong, climate has a positive effect, and the growth effects are minor; in the Brahmaputra, climate has a slightly negative, almost neutral effect, while growth is more extreme—especially in terms of UWR changes.

3.6 Populations at Risk to Increased Water Stress

An analysis was performed to assess the population that is prone to water-stress exposure under current conditions and future scenarios. The population of each ASR was assigned to one of the water-stress classifications, using both UWR and WSI, based on the value of the resulting water stress indicator. Note that in our model we are assuming that population growth is constant by EPPA region, where each ASR grows proportionally to the baseline population. For UWR, a simple classification is used: Class 1 is less than 5%, class 2 is between 5% and 10%, classes 3, 4 and 5 are set at increments of ten, and the final class, 6, is set to values above 40%. We count the number of people in each UWR class for the Baseline scenario and compare that to the same metric at 2050 from the three scenario ensembles (*Just Climate*, *Just Growth*, and *Climate and Growth*). These results are shown in **Figure 31**.

In this figure, note that the *Just Climate* ensemble has no population growth, so the difference between the *Just Climate* and the other two ensembles is largely attributed to the additional population (in the *Just Growth* and *Climate and Growth* scenarios). Also, note that the *Just Climate* ensemble does not change in the extreme classes: Class 1, 5 and 6. The largest effect of climate is to shift population from Class 2 to Class 3 (see **Table 1a**), which is a movement into a more severe water stress state. We see this movement in *Just Growth* as well (**Table 1b**), but here the unmet requirement is changing for many ASRs from Classes 2 and 3 into the next higher stress class (Classes 3 and 4, respectively). These ASRs are moving into a higher UWR class because growth only increases UWR, as we have shown (Section 3.5). The most striking change is the increase of population in Class 4 and Class 6, compared to the baseline, for both the *Just Growth* and *Climate and Growth* ensembles. The increases in Class 6 are largely attributed to population growth occurring within ASRs that are already at this high stress level (**Tables 1b and 1c**); increases in Class 4 populations are largely attributed to the addition of former Class 3 populations, due to water demand increases from growth (Table 1b) or the combined effects of growth and climate change on supply and demand changes (Table 1c). An additional notable result of the *Climate and Growth* scenario is that it removes all instances of populations moving to decreased stressed conditions, seen in a small fraction of cases for the *Just Climate* scenario (**Tables 1a and 1c**).

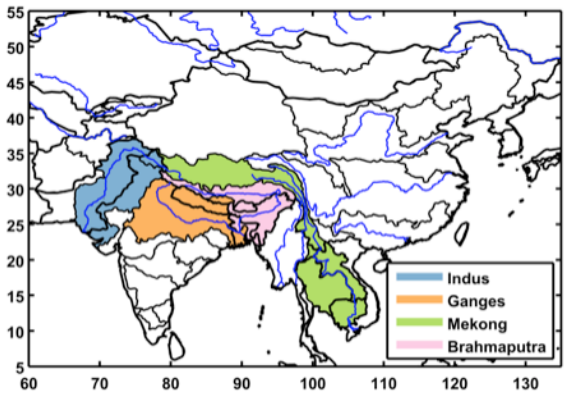

Figure 29. Map of major basins used to show the aggregate frequency distributions of water stress.

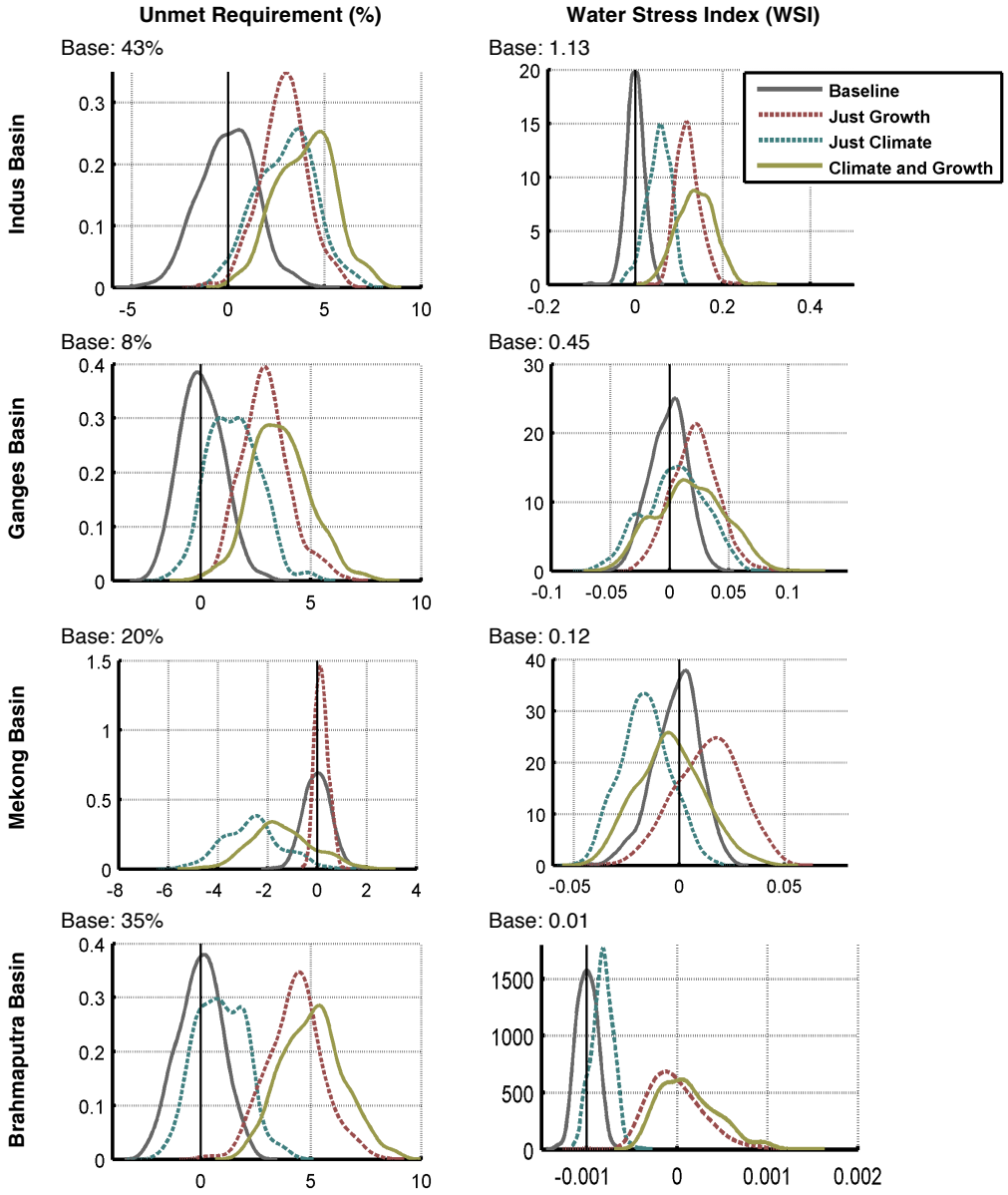

Figure 30. As in Fig. 29, but aggregated over selected basins (Fig. 30). Mean baseline value shown above each figure. Results are shown for the Just Growth, Just Climate, and Climate and Growth ensemble scenarios.

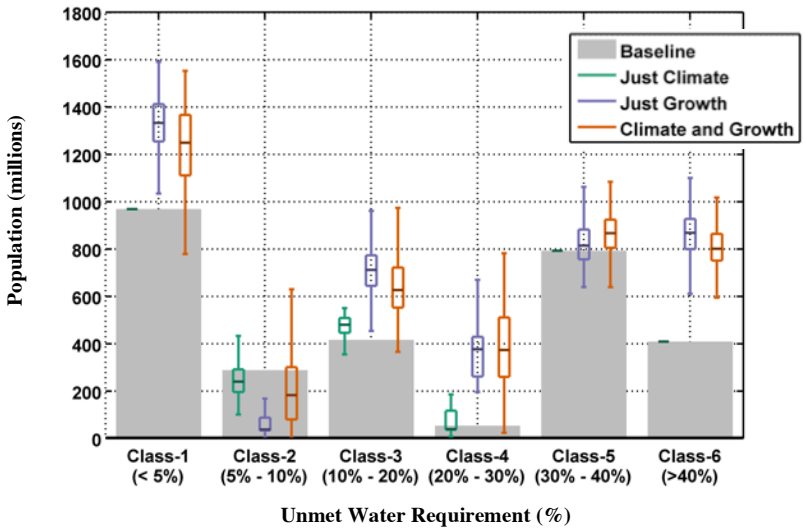

Figure 31. Population exposed to water stress based on UWR classifications using the 2041–2050 mean. Grey bars represent the number of people in each class in the baseline scenario (set to year-2000 value); the box-and-whisker plots show the distributional characteristics of the three ensemble scenarios..

Table 1. Matrix of populations' (in millions) exposure to water stress. Shaded gray cells show the population remaining in the UWR class relative to the Baseline result. The off-diagonal cells denote population shifts by 2050 across the various UWR classes; population shifts between classes are depicted by their location within the table matrix. Each cell provides the 10th [left, bracketed], 50th (center, bold), and 90th [right, bracketed] percentile results.

1a. Just Climate

From \ To	Class-1	Class-2	Class-3	Class-4	Class-5	Class-6
Class-1	[848] **970** [970]	[0] **0** [122]				
Class-2		[124] **197** [197]	[93] **93** [167]			
Class-3		[0] **44** [44]	[294] **372** [372]	[0] **0** [78]		
Class-4			[15] **15** [47]	[8] **39** [39]		
Class-5					[793] **793** [793]	
Class-6					[0] **0** [3]	[406] **409** [409]

1b. Just Growth

From \ To	Class-1	Class-2	Class-3	Class-4	Class-5	Class-6
Class-1	[1188] **1332** [1477]	[0] **0** [66]				
Class-2		[29] **36** [117]	[227] **273** [401]	[0] **124** [162]		
Class-3			[344] **415** [464]	[198] **238** [313]		
Class-4				[27] **32** [37]	[0] **0** [43]	[0] **43** [51]
Class-5					[703] **806** [925]	[103] **216** [252]
Class-6						[556] **624** [691]

1c. Climate and Growth

From \ To	Class-1	Class-2	Class-3	Class-4	Class-5	Class-6
Class-1	[978] **1249** [1422]	[0] **62** [346]				
Class-2		[1] **36** [145]	[216] **272** [394]	[0] **127** [162]		
Class-3		[0] **55** [76]	[253] **336** [469]	[125] **296** [367]		
Class-4				[26] **31** [35]	[0] **4** [48]	[0] **41** [51]
Class-5					[742] **851** [963]	[117] **141** [227]
Class-6						[560] **621** [696]

For WSI, water-stress classifications are based on the aforementioned Smakhtin *et al.* (2005) study (Section 2.4): $WSI < 0.3$ is slightly exploited; $0.3 \leq WSI \leq 0.6$ is moderately exploited; $0.6 \leq WSI \leq 1$ is heavily exploited; $1 \leq WSI < 2$ is overly exploited; and $WSI \geq 2$ is extremely exploited. The strongest effect of the *Just Climate* scenario is to bring more populations currently living under Moderately stressed conditions into Heavily water stressed environments by 2050 (**Figure 33**, **Table 2a**). Similar to the results seen for UWR, there are only a small number of cases in which climate will move populations into less stressed WSI conditions. The effect of *Just Growth* is consonant with the *Just Climate* result (**Table 2b**), where a comparable increase in population is taken from Moderately into Heavily stressed conditions. Combined, the *Climate and Growth* scenario places comparable populations from Moderately stressed environments into Heavily stressed environments (Figure 33, **Table 2c**). In doing so, the Moderately stressed condition is the only class of WSI that contains a decrease in the median total population (on the order of 100 million) at 2050 (compared to the Baseline condition).

We further aggregate these classifications to underscore the impacts of these scenarios on the more severe water-stress conditions. We assign a threshold to both the UWR and WSI measures, so an ASR may be classified as either stressed (over the threshold) or unstressed (under the threshold). The developed aggregations are shown in **Table 3**. For UWR we use a threshold value of 10% (reflecting at least 10% annual water requirements not met) and for WSI we use a threshold value of 0.6 (must be at least in the Heavily stressed class). Overall, we find no occurrences (in any member, among all scenarios) of a decrease in the total water-stressed population by 2050. The effect of socio-economic growth is quite evident, as seen by the median result of over 1 billion additional people exposed to "water-stressed" conditions by 2050. Additionally, in only 10% of the members will this result be below 750 million based on either the UWR or WSI indicators. The *Just Climate* scenario impact is small for the UWR-based result, causing a median shift of less than 2% population increase. Population shifts across the WSI-based threshold are almost ten times more sensitive to the *Just Climate* scenario compared to the UWR-based result, with nearly 400 million additional people becoming water-stressed by 2050. The *Just Growth* scenario provides very comparable results between the UWR and WSI based thresholds, with both outcomes indicating that over 1 billion additional people by 2050 will become water-stressed due to socioeconomic growth unconstrained by global actions to limit greenhouse gas concentrations. There is a small beneficial effect to this result when the effects of climate change are added (as indicated by the *Climate and Growth* result), but it only results in a ~1% reduction in the population growth affected by socioeconomic changes. Overall, the central tendency of the UWR and WSI based thresholds in the *Climate and Growth* scenario is to flank (i.e. within ± 100 million) a future outcome that 1 billion additional people will be living in regions under water stress.

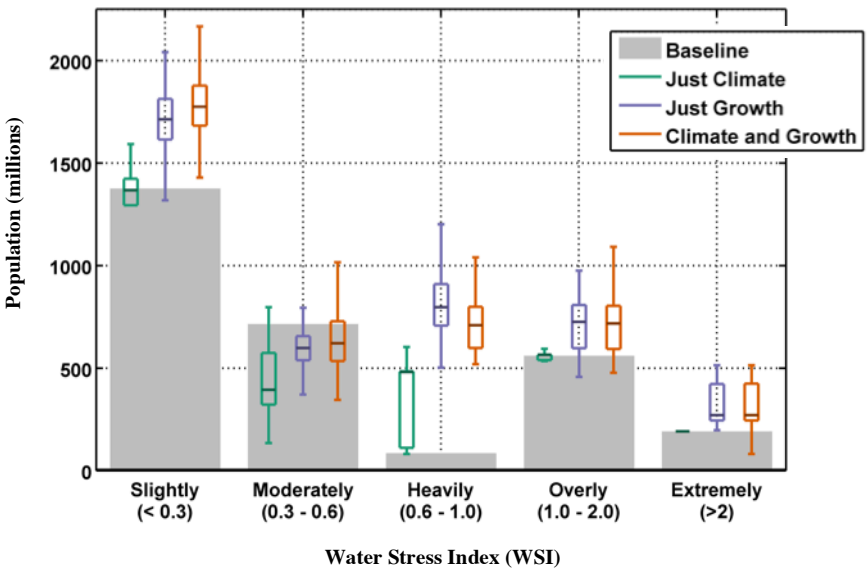

Figure 32. Population exposed to water stress based on WSI classifications using the 2041–2050 mean. Grey bars represent the number of people in each class in the baseline scenario (set to year-2000 value); the box-and-whisker plots show the distributional characteristics of the three ensemble scenarios.

Table 2. Matrix of populations' (in millions) exposure to water stress. Shaded gray cells show the population remaining in the WSI class relative to the Baseline result. The off-diagonal cells denote population shifts by 2050 across the various WSI classes; population shifts between classes are depicted by their location within the table matrix. Each cell provides the 10th [left, bracketed], 50th (center, bold), and 90th [right, bracketed] percentile results.

2a. Just Climate

From \ To	Slightly	Moderately	Heavily	Overly	Extremely
Slightly	[1296] **1296** [1296]	[82] **82** [82]			
Moderately	[0] **73** [216]	[153] **313** [586]	[0] **395** [402]		
Heavily			[82] **82** [86]	[0] **4** [4]	
Overly			[0] **0** [26]	[535] **562** [562]	
Extremely					[163] **192** [192]

2b. Just Growth

From \ To	Slightly	Moderately	Heavily	Overly	Extremely
Slightly	[1531] **1713** [1875]	[135] **177** [318]			
Moderately		[253] **368** [534]	[546] **699** [889]		
Heavily			[9] **107** [124]	[21] **25** [102]	
Overly				[529] **699** [810]	[0] **0** [207]
Extremely					[221] **246** [270]

2c. Climate and Growth

From \ To	Slightly	Moderately	Heavily	Overly	Extremely
Slightly	[1589] **1736** [1904]	[104] **161** [277]			
Moderately	[0] **0** [123]	[323] **443** [987]	[13] **625** [746]		
Heavily			[0] **107** [137]	[7] **29** [127]	
Overly				[524] **679** [805]	[0] **0** [207]
Extremely					[207] **244** [270]

Table 3. Water-stressed population increase (in millions and percent). Based on a threshold of 10% for unmet requirement (UWR) and 0.6 for WSI. Each cell provides the 10th percentile [left bracketed value], median (center in bold type), and 90th percentile [right bracketed value] results.

	Potential Increase in Population in water stressed regions (millions)					
	UWR > 10% *Baseline = 1672 (57%)*			*WSI > 0.6* *Baseline = 839 (28.6%)*		
	10th	**Median**	90th	10th	**Median**	90th
Just Climate	[4]	**49**	[122]	[0]	**395**	[402]
	[0.1%]	**1.7%**	[4.2%]	[0%]	**13.5%**	[13.7%]
Just Growth	[818]	**1,086**	[1,297]	[784]	**1,001**	[1,242]
	[21.8%]	**26.0%**	[29.2%]	[20.1%]	**23.9%**	[28.1%]
Climate and Growth	[757]	**1,030**	[1,264]	[297]	**911**	[1,090]
	[19.8%]	**25.1%**	[28.9%]	[7.3%]	**22.1%**	[24.7%]

4. DISCUSSION AND CLOSING REMARKS

This study has employed the IGSM-WRS framework aimed at assessing the fate of managed water systems, depicted by 52 large sub-regions across Asia. A number of experiments were performed to assess the isolated as well as combined effects of socioeconomic growth and regional climate change out through the 2040s. With this large ensemble of projections, a frequency distribution of impacts was developed that articulates the severity and likelihood of water stress in this region of Asia. We find a variety of patterns across the region for changes in surface-freshwater supply, and this results from a variety of influences in the hydroclimate (i.e. runoff) as well as water requirements in agriculture, industry and municipality water needs. We find that regions most vulnerable to changes in climate include much of China (especially in the north), Pakistan and Afghanistan. Further, India, China and Mainland Southeast Asia are all highly likely to experience significant changes in socioeconomically-driven water requirements.

Some limitations and assumptions made within the framework for this particular experimentation are notable. First, we model *consumptive* water requirement rather than withdrawal. We do this because our sub-regions are large, and presumably will include substantial water reuse within an ASR. Second, we keep irrigated areas constant by crop for all scenarios. In reality, these changes respond to a variety of drivers, including local and global food prices, land and water availability, and government subsidies. Estimating changes in irrigated area is a difficult task; however, we do plan to include these changes in an upcoming report, as they have the potential for profound impact on future water stress. Third, the framework uses socioeconomic drivers exogenously, therefore missing potentially important feedbacks (e.g., water limitations could have an adverse effect on food or energy prices, which would likely cause shocks in the economic system on a local or global scale, further affecting investments in water-related technology and infrastructure). Lastly, this framework's water management simulation uses a single objective function with perfect foresight within a calendar

year, consistent priorities across all ASRs, and perfect cooperation within a river network. Furthermore, we do not simulate hydropower generation in the representative reservoirs. Realistic water management is done in a complicated, often inefficient fashion with varying knowledge about next month's water supply (e.g., water managers generally know historical averages). These assumptions about water management allow us to have a water allocation scheme that is consistent across ASR and scenario, providing a model environment that is not partial to regions that are historically "better" water managers. Our scheme also adapts to changes in water supply and requirement more efficiently than a realistic system, likely providing a more optimistic picture of water stress in the region. For example, water managers are typically challenged and forced to make operational decisions based on imperfect information and forecasts, and hydropower needs may interfere with water allocation. These assumptions and limitations are issues we plan to address in future studies.

Regardless, there are a number of significant results we have found in this study. For example, by isolating socioeconomic growth from changes in climate, we find that the two have characteristically different impacts on water stress. Industrial and municipal water requirements, driven by socioeconomic growth, are less significant in the baseline but *will* increase considerably in the future. Alternatively, changes in climate can be significant in our current system, but do not change as much (compared to growth) in the future relative to their baseline value, and these changes range from positive to negative. Socioeconomic drivers on water requirements are, therefore, likely to play a larger role in future management decisions than they do in the current system. When we assess potential population increase in water stressed regions, we find it highly probable that many people who live in moderately stressed conditions will live in heavily stressed conditions in the future. We specifically find that increases in water-stressed populations will be almost 1 billion in the median case, more than doubling the baseline case (for WSI). These changes will likely require more aggressive water policies and regulations in areas where water resource decisions have been less tense historically. Without assertive water policies in these regions, water limitations could be harmful to the health and well being of the people in these regions, as well as the environment.

These results do not necessarily imply an insurmountable future for this region. Through climate mitigation, and perhaps most importantly, proper planning and financing of adaptive and protective measures for these anticipated shortages—based on reliable information as to the effectiveness of certain strategies to avert the risks presented above—these future water systems can be augmented to better ensure their resiliency and sustainability. Addressing these options for the future, however, will require substantial research and additional experimentation with integrative tools like the IGSM-WRS. Forthcoming studies will expand upon these experiments to quantify the effectiveness of climate mitigation policies and widespread adaptive measures such as enhanced storage, expansive water transfers, water-use efficiencies, and reduced consumption via water mandates or changes in common practice.

Acknowledgments
The Joint Program on the Science and Policy of Global Change is funded by the U.S. Department of Energy, Office of Science under grants DE-FG02-94ER61937, DE-FG02-93ER61677, DE-FG02-08ER64597, and DE-FG02-06ER64320; the U.S. Environmental Protection Agency under grants XA-83344601-0, XA-83240101, XA-83042801-0, PI-83412601-0, RD-83096001, and RD-83427901-0; the U.S. National Science Foundation under grants SES-0825915, EFRI-0835414, ATM-0120468, BCS-0410344, ATM-0329759, and DMS-0426845; the U.S. National Aeronautics and Space Administration under grants NNX07AI49G, NNX08AY59A, NNX06AC30A, NNX09AK26G, NNX08AL73G, NNX09AI26G, NNG04GJ80G, NNG04GP30G, and NNA06CN09A; the U.S. National Oceanic and Atmospheric Administration under grants DG1330-05-CN-1308, NA070AR4310050, and NA16GP2290; the U.S. Federal Aviation Administration under grant 06-C-NE-MIT; the Electric Power Research Institute under grant EP-P32616/C15124; and a consortium of 40 industrial and foundation sponsors (for the complete list see http://globalchange.mit.edu/sponsors/all).

5. REFERENCES

Alcamo, J., M. Flörke and M. Märker, 2007: Scenarios of global water resources: What are the effects of socio-economic drivers as compared to climate change? *Hydrological Science Journal*, 52, 247–275.

Alcamo, J., M. Florke and M. Märker, 2010: Future long-term changes in global water resources driven by socio-economic and climate changes. *Hydrologic Sciences-Journal-des Sciences Hydrologiques*, 52(2).

Arndt, C., C. Fant, S. Robinson and K. Strzepek, 2014: Informed selection of future climates. *Climatic Change.* Manuscript in preparation.

Arnell, N.W., D.P. van Vuuren and M. Isaac, 2011: The implications of climate policy for the impacts of climate change on global water resources. *Global Environmental Change*, 21(2), 592–603.

Blanc, É., K. Strzepek, C.A. Schlosser, H. Jacoby, A. Gueneau, C. Fant, S. Rausch and J. Reilly, 2013: Analysis of U.S. water resources under climate change, *Earth's Future*, 2: 197–224, doi: 10.1002/2013EF000214.

Fant, C,. A. Gueneau, K. Strzepek, S. Awadalla, W. Farmer, É. Blanc and C.A. Schlosser, 2012: CliCrop: A crop water-stress and irrigation demand model for an integrated global assessment modeling approach. MIT JPSPGC *Report 214*, April, 26 p. (http://globalchange.mit.edu/files/document/MITJPSPGC_Rpt214.pdf).

FAO (Food and Agriculture Organization of the United Nations), 2013: *FAO Statistical Yearbook 2013 - World Food and Agriculture*, FAO, Rome, Italy, 307 pp, ISBN 978-92-5-107396-4.

Forest, C. E., P. H. Stone and A. P. Sokolov, 2008: Constraining climate model parameters from observed 20th century changes. *Tellus*, 60A, 911–920.

Georgakakos, A., P. Fleming, M. Dettinger, C. Peters-Lidard, T.C. Richmond, K. Reckhow, K. White and D. Yates, 2014: Ch. 3: Water Resources. Climate Change Impacts in the *United States: The Third National Climate Assessment*, J.M. Melillo, T.C. Richmond and G.W. Yohe, Eds., U.S. Global Change Research Program, 69–112, doi:10.7930/ J0G44N6T.

Hargreaves G. and R. Allen, 2003: History and evaluation of Hargreaves evapotranspiration equation, *J Irrig Drain E-Asce*, 129: 53–63.

Huffman, G.J., R.F. Adler, D.T. Bolvin and G. Gu, 2009: Improving the Global Precipitation Record: GPCP Version 2.1 *Geophys. Res. Lett.,* 36, L17808.

Jiménez Cisneros, B.E., T. Oki, N.W. Arnell, G. Benito, J.G. Cogley, P. Döll, T. Jiang and S.S. Mwakalila, 2014: Freshwater resources. In: *Climate Change 2014: Impacts, Adaptation, and Vulnerability. Part A: Global and Sectoral Aspects.* Contribution of Working Group II to the Fifth Assessment Report of the Intergovernmental Panel on Climate Change [Field, C.B., V.R. Barros, D.J. Dokken, K.J. Mach, M.D. Mastrandrea, T.E. Bilir, M. Chatterjee, K.L. Ebi, Y.O. Estrada, R.C. Genova, B. Girma, E.S. Kissel, A.N. Levy, S. MacCracken, P.R. Mastrandrea and L.L. White (eds.)]. Cambridge University Press, Cambridge, United Kingdom and New York, NY, USA.

Kumar, R.K., A.K. Sahai, K.K. Kumar, S.K. Patwardhan, P.K. Mishra, J.V. Revadekar, K. Kamala and G.B. Pant, 2006: High-resolution climate change scenarios for India for the 21st century. *Current Science*, 90 (3): 334–245.

Lall, U. and A. Sharma, 1996: A nearest neighbor bootstrap for resampling hydrologic time series, *Water Resources Research*, 32, 679–693.

Meehl, G.A., C. Covey, T. Delworth, M. Latif, B. McAvaney, J.F.B. Mitchell, R.J. Stouffer and K.E. Taylor, 2007: The WCRP CMIP3 multi-model dataset: A new era in climate change research. *Bull. Amer. Met. Soc*., 88: 1383–1394.

O'Brien, K., R. Leichenko, U. Kelkar, H. Venema, G. Aandahl, H. Tompkins, A. Javed, S. Bhadwal, S. Barg, L. Nygaard, J. West, 2004: Mapping vulnerability to multiple stressors: climate change and globalization in India. *Global Environmental Change*, 14(4): 303–313

Oleson K.W., G.Y. Niu, Z.L. Yang, D.M. Lawrence, P.E. Thornton, P.J. Lawrence, R. Stöckli, R.E. Dickinson, G.B. Bonan, and S. Levis, 2008: Improvements to the Community Land Model and their impact on the hydrological cycle *J*. *Geophys*. *Res*. 113 G01021.

Paltsev, S., J.M. Reilly, H.D. Jacoby, R.S. Eckaus, J. McFarland, M. Sarofim, M. Asadoorian and M. Babiker, 2005: The MIT Emissions Prediction and Policy Analysis (EPPA) Model: Version 4. MIT JPSPGC *Report 125*, August, 72 p. (http://globalchange.mit.edu/files/document/MITJPSPGC_Rpt125.pdf).

Piao, S., P. Ciais, Y. Huang, Z. Shen, S. Peng, J. Li, L. Zhou, H. Liu, Y. Ma, Y. Ding, P. Friedlingstein, C. Liu, K. Tan, Y. Yu, T. Zhang and J. Fang, 2010: The impacts of climate change on water resources and agriculture in China. *Nature* 467, 43–51, doi:10.1038/nature09364.

Ramirez-Villegas, J. and A. Jarvis, 2010: Downscaling global circulation model outputs: the delta method decision and policy analysis working paper No. 1. *Decision and Policy Analysis Working Papers.* International Center for Tropical Agriculture (CIAT), Cali, Colombia.

Rosegrant, M., C. Ringler, S. Msangi, T. Sulser, T. Zhu and S. Cline, 2008: *International Model for Policy Analysis of Agricultural Commodities and Trade (IMPACT): Model Description*, International Food Research Institute: Washington, D.C.

Schlosser, C.A., X. Gao, K. Strzepek, A. Sokolov, C.E. Forest, S. Awadalla and W. Farmer, 2012: Quantifying the likelihood of regional climate change: A hybridized approach. *Journal of Climate*, 26(10): 3394–3414, doi: 10.1175/JCLI-D-11-00730.1.

Sheffield, J., G. Goteti and E.F. Wood, 2006: Development of a 50-year high-resolution global dataset of meteorological forcings for land surface modeling. *J. Climate*, 19: 3088-3111.

Shen, Y., T. Oki, N. Utsumi, S. Kanae and N. Hanasaki, 2008: Projection of future world water resources under SRES scenarios: water withdrawal. *Hydrological Science Journal*, 53, 11–33.

Siebert, S., V. Henrich, K. Frenken and J. Burke, 2013: Update of the digital Global Map of Irrigation Areas (GMIA) to Version 5, *Institute of Crop Science and Resource Conservation*, Rheinische Friedrich-Wilhelms-Universität Bonn, Germany, 171 pp.

Siebert, S., P. Doll, J. Hoogeveen, J.-M. Faures, K. Frenken and S. Feick, 2005: Development and validation of the global map of irrigation, *Hydrol. and Earth Sys. Sci.*, 9, 535–547. SRef-ID: 1607-7938/hess/2005-9-535.

Smakhtin, V., C. Revanga and P. Doll, 2005: Taking into account environmental water requirements in global scale water resources assessments. (http://www.iwmi.cgiar.org/assessment/files/pdf/publications/researchreports/carr2.pdf).

Sokolov, A.P., C.A. Schlosser, S. Dutkiewicz, S. Paltsev, D.W. Kicklighter, H.D. Jacoby, R.G. Prinn, C.E. Forest, J.M. Reilly, C. Wang, B. Felzer, M.C. Sarofim, J. Scott, P.H. Stone, J.M. Melillo and J. Cohen, 2005: The MIT Integrated Global System Model (IGSM) Version 2: Model description and baseline evaluation. MIT JPSPGC *Report 124*, July, 40 p. (http://globalchange.mit.edu/files/document/MITJPSPGC_Rpt124.pdf).

Sokolov, A.P., P.H. Stone, C.E. Forest, R.G. Prinn, M.C. Sarofim, M. Webster, S. Paltsev, C.A. Schlosser, D. Kicklighter, S. Dutkiewicz, J. Reilly, C. Wang, B. Felzer, J. Melillo and H.D. Jacoby, 2009. Probabilistic Forecast for 21st Century Climate Based on Uncertainties in Emissions (without Policy) and Climate Parameters, *Journal of Climate,* 22(19): 5175-5204 (doi: 10.1175/2009JCLI2863.1).

Strzepek, K., A. McCluskey, B. Boehlert, M. Jacobsen and C. Fant, 2011: Climate variability and change: a basin scale indicator approach to understanding the risk to water resources development and management. Water papers. Washington, DC: World Bank (http://documents.worldbank.org/curated/en/2011/09/15897484/climate-variability-change-basin-scale-indicator-approach-understanding-risk-water-resources-development-management).

Strzepek, K., C.A. Schlosser, A. Gueneau, X. Gao, É. Blanc, C. Fant, B. Rasheed and H. Jacoby, 2013: Modeling water resource systems under climate change: IGSM-WRS. *J. Adv. Earth Model Sys.* 5(3): 638–653.

Tchakaloff, V., 1957: Formules de cubatures mécaniques à coefficients non negatifs. *Bull Sci Math* 81: 123–34.

Thenkabail, P.S., C.M. Biradar, P. Noojipady, V. Dheeravath, Y.J. Li, M. Velpuri, G.P.O. Reddy, X.L. Cai, M. Gumma, H. Turral, J. Vithanage, M. Schull and R. Dutta, 2008: *A Global Irrigated Area Map (GIAM) using remote sensing at the end of the last millennium*, International Water Management Institute, 63 pp. (http://www.iwmigiam.org/info/gmi-doc/GIAM-world-book.pdf).

Vörösmarty, C.J., P. Green, J. Salisbury and R.B. Lammers, 2000: Global water resources: vulnerability from climate change and population growth. *Science*, 289, 284–288.

WCOD (World Commission on Dams), 2000: *Dams and Development: A New Framework for Decision-Making - The Report of the World Commission on Dams*, Earthscan Publications, London, England, 356 pp.

Webster, M.D., S. Paltsev, J. Parsons, J. Reilly and H. Jacoby, 2008: Uncertainty in Greenhouse Emissions and Costs of Atmospheric Stabilization, MIT JPSPGC *Report 165* (http://globalchange.mit.edu/files/document/MITJPSPGC_Rpt165.pdf)

Webster, M., A.P. Sokolov, J.M. Reilly, C.E. Forest, S. Paltsev, A. Schlosser, C. Wang, D. Kicklighter, M. Sarofim, J. Melillo, R.G. Prinn and H.D. Jacoby, 2012. Analysis of climate policy targets under uncertainty, *Climatic Change*, 112(3-4) 569–583.

Wei, X., C. Declan, L. Erda, X. Yinlong, J. Hui, J. Jinhe, H. Ian and L. Yan (2009) Future cereal production in China: The interaction of climate change, water availability and socio-economic scenarios. *Global Environmental Change* Vol. 19(1): 34–44.

Willmott, C.J., and J.J. Feddema, 1992: A more rational climatic moisture index. *Prof. Geographer*, 1: 84–88, doi: 10.1111/j.0033-0124.1992.00084.x.

APPENDIX A: CLIMATE-CHANGE PATTERN KERNELS

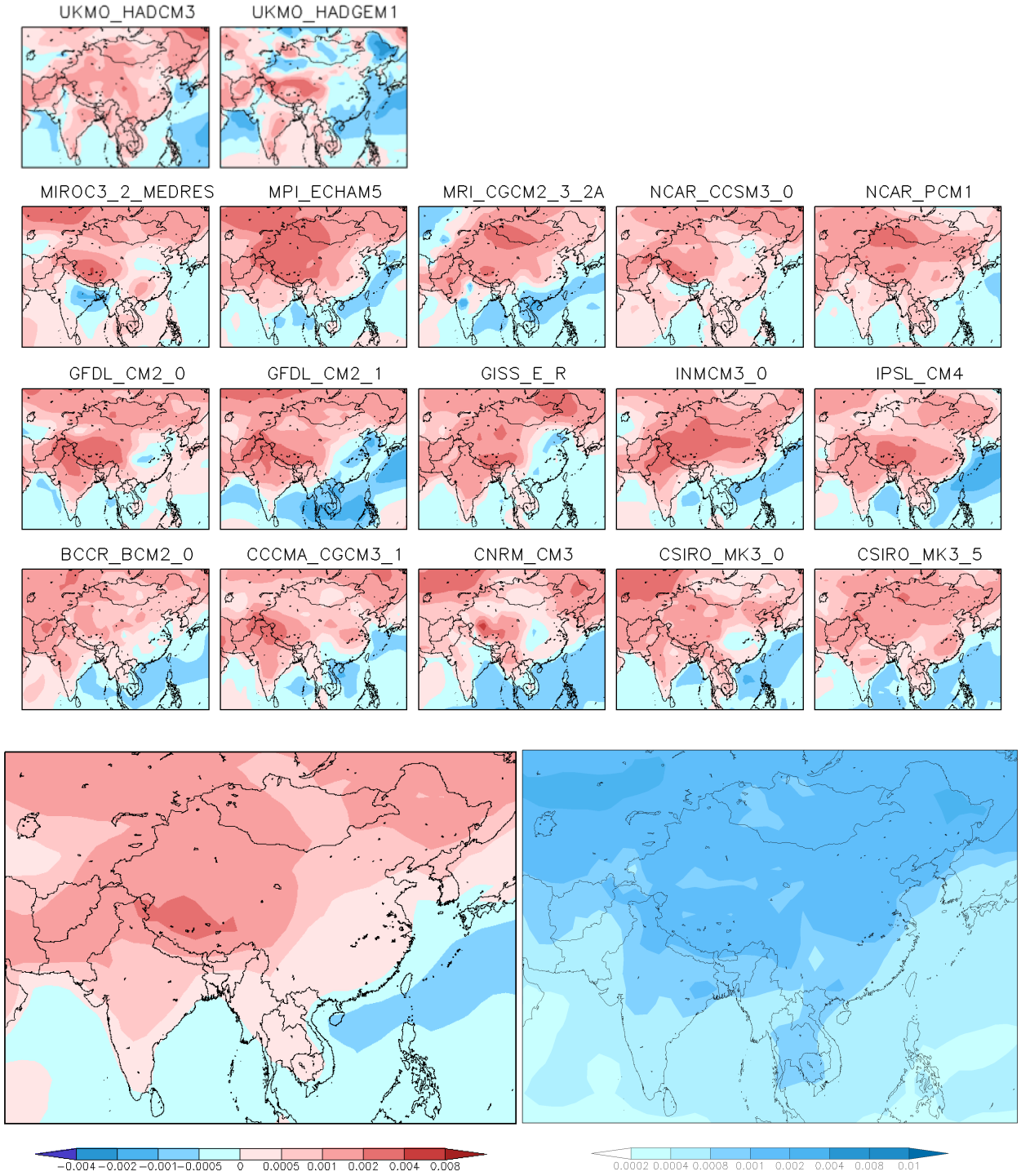

Figure A-1. Climate-change pattern kernels (unitless) of DJF temperature from the IPCC AR4 climate models. Used to construct hybrid climate-change distributions from the IGSM. Shown are the relative changes in DJF temperature in response to a unit global temperature increase as a result of anthropogenic greenhouse emissions. Top: 17-map series showing pattern kernels for each AR4 GCM. Bottom left: mean of the pattern kernels. Bottom right: standard deviation.

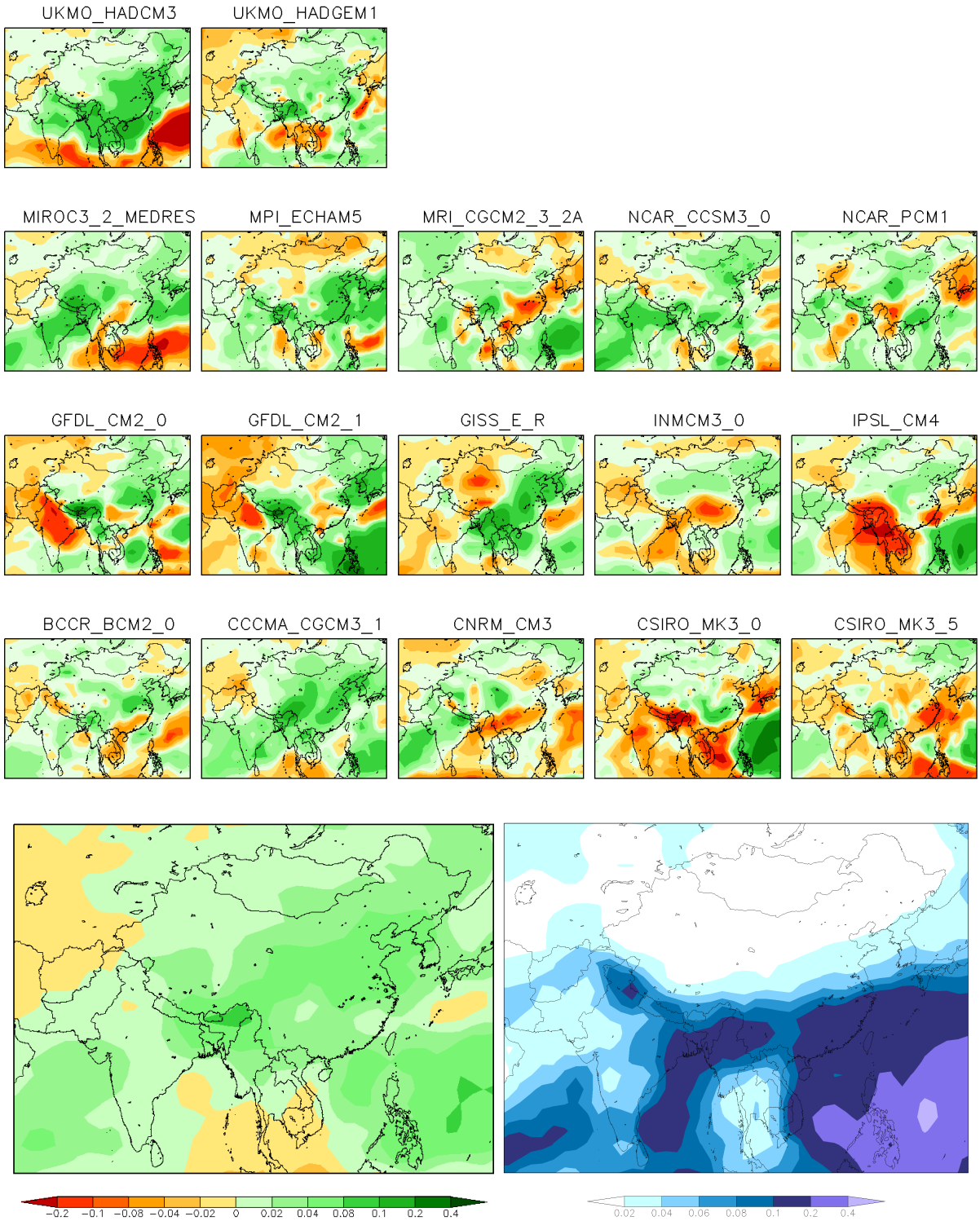

Figure A-2. Climate-change pattern kernels (unitless) of DJF precipitation from the IPCC AR4 climate models. Used to construct hybrid climate-change distributions from the IGSM. Shown are the relative changes in DJF precipitation in response to a unit global temperature increase as a result of anthropogenic greenhouse emissions. Top: 17-map series showing pattern kernels for each AR4 GCM. Bottom left: mean of the pattern kernels. Bottom right: standard deviation.

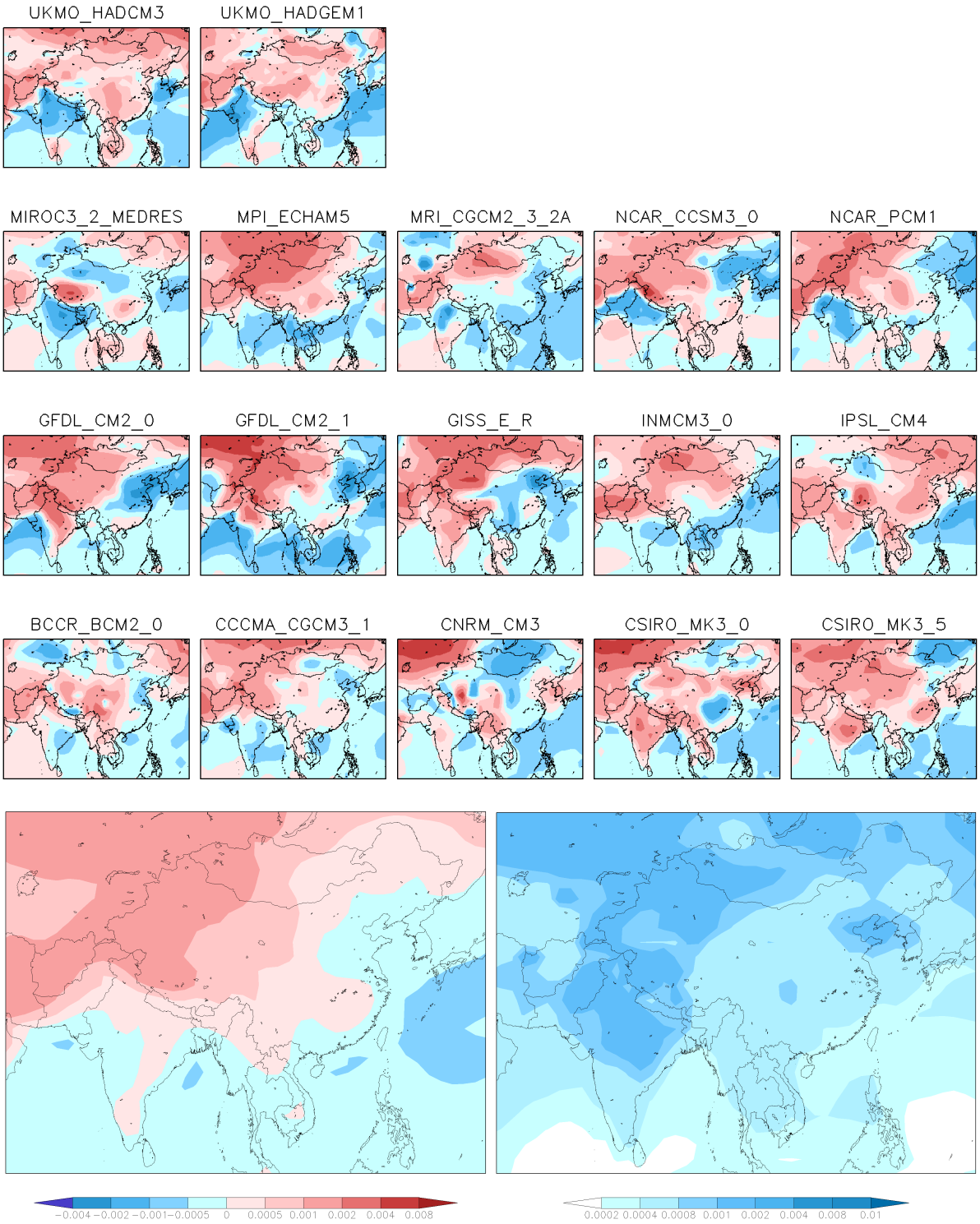

Figure A-3. Climate-change pattern kernels (unitless) of JJA temperature from the IPCC AR4 climate models. Used to construct hybrid climate-change distributions from the IGSM. Shown are the relative changes in JJA temperature in response to a unit global temperature increase as a result of anthropogenic greenhouse emissions. Top: 17-map series showing pattern kernels for each AR4 GCM. Bottom left: mean of the pattern kernels. Bottom right: standard deviation.

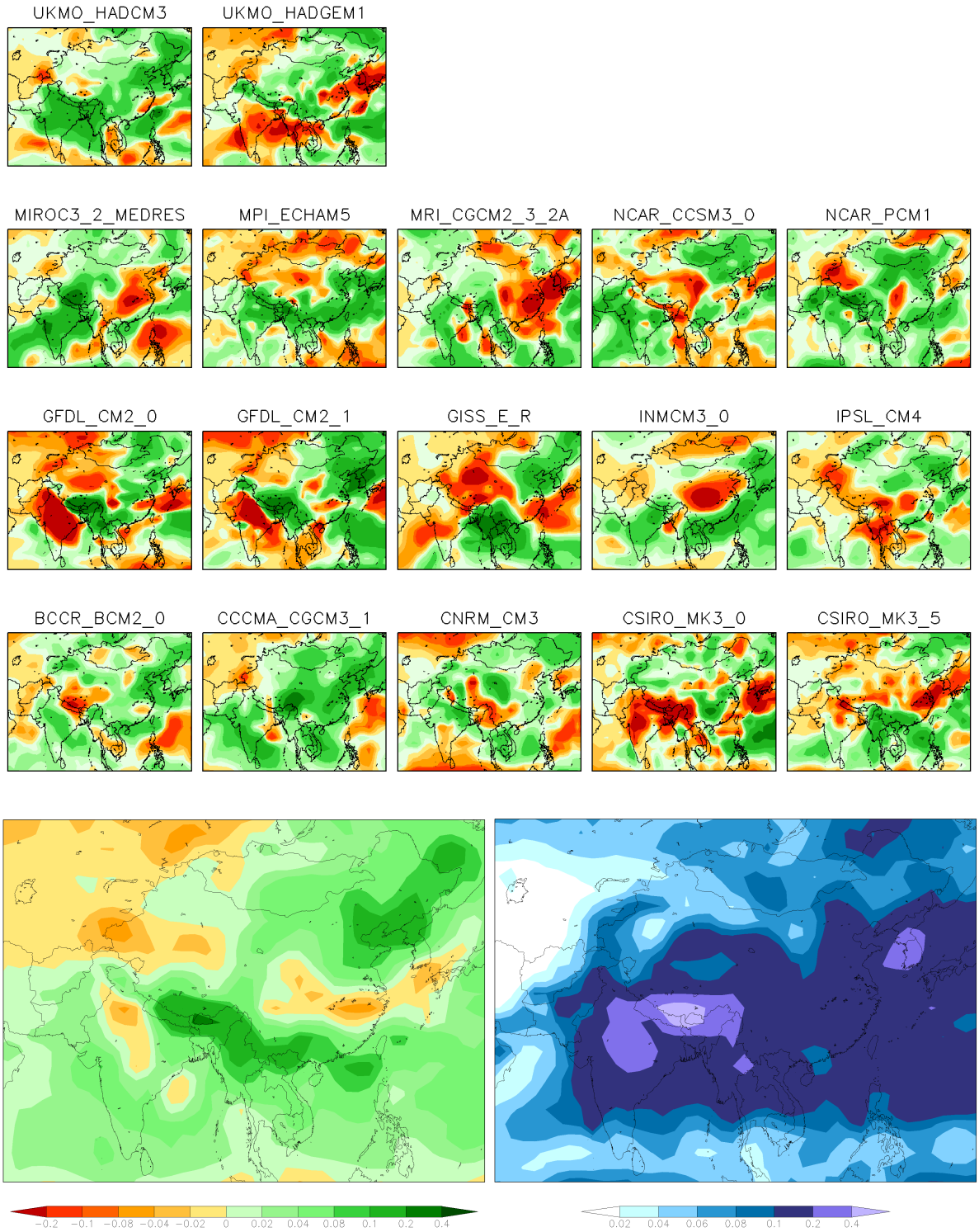

Figure A-4. Climate-change pattern kernels (unitless) of JJA precipitation from the IPCC AR4 climate models. Used to construct hybrid climate-change distributions from the IGSM. Shown are the relative changes in JJA precipitation in response to a unit global temperature increase as a result of anthropogenic greenhouse emissions. Top: 17-map series showing pattern kernels for each AR4 GCM. Bottom left: mean of the pattern kernels. Bottom right: standard deviation.

APPENDIX B: UNMET WATER REQUIREMENT SINGLE MATRIX AND MAPS

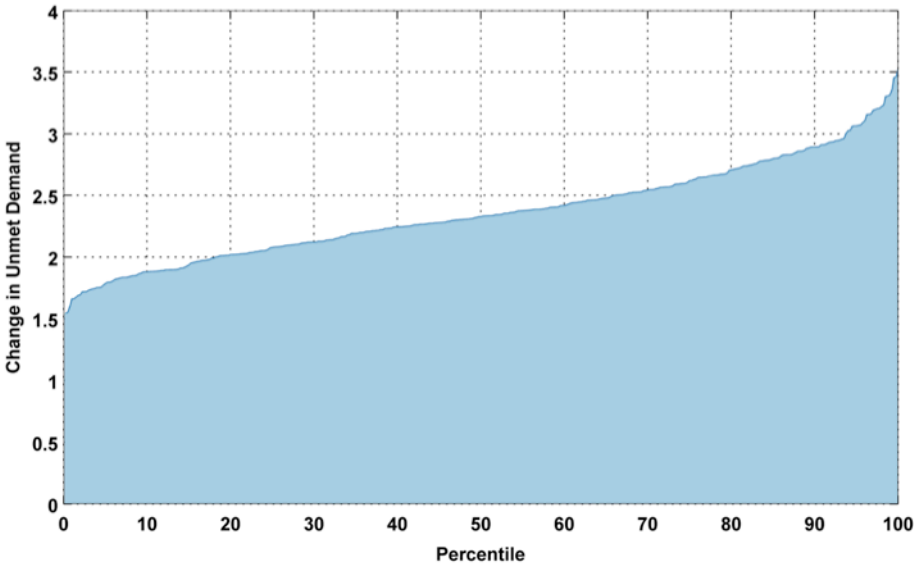

Figure B-1. Population weighted change in UWR (%) across the region for the *Just Growth* ensemble.

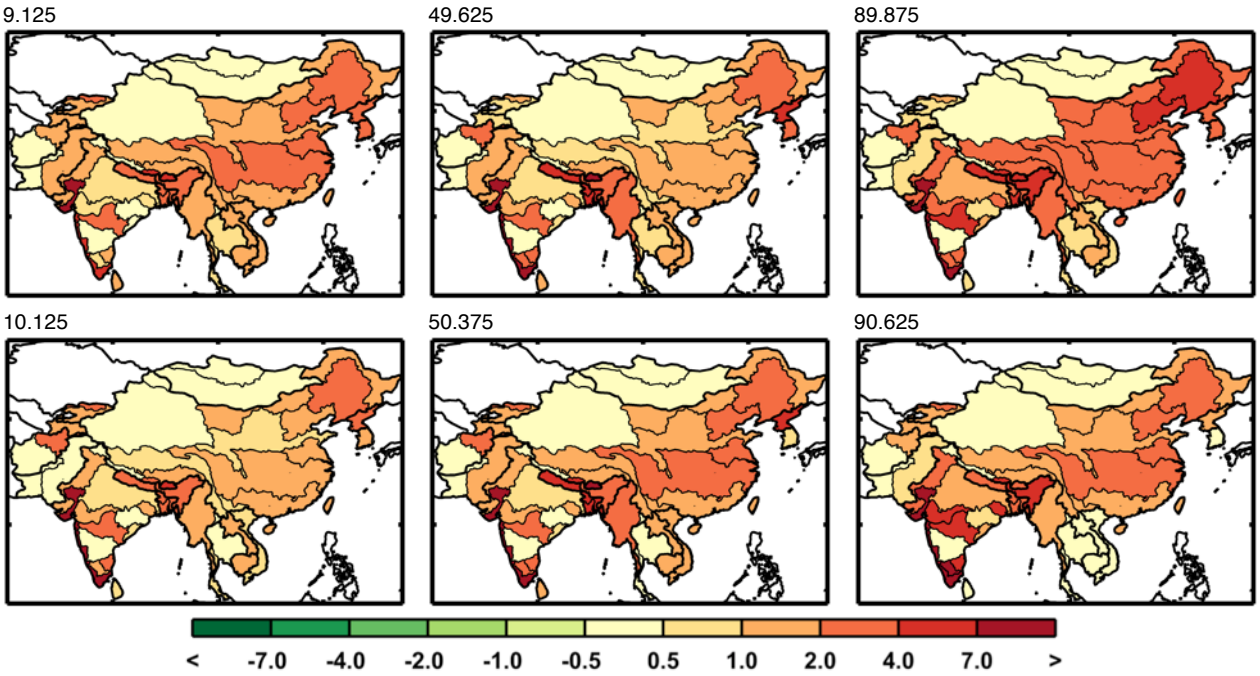

Figure B-2. UWR change for the *Just Growth* ensemble (in %) patterns around the 10th, 50th, and 90th percentile, two each, based on the mean UWR change for the region. Top label shows the percentile.

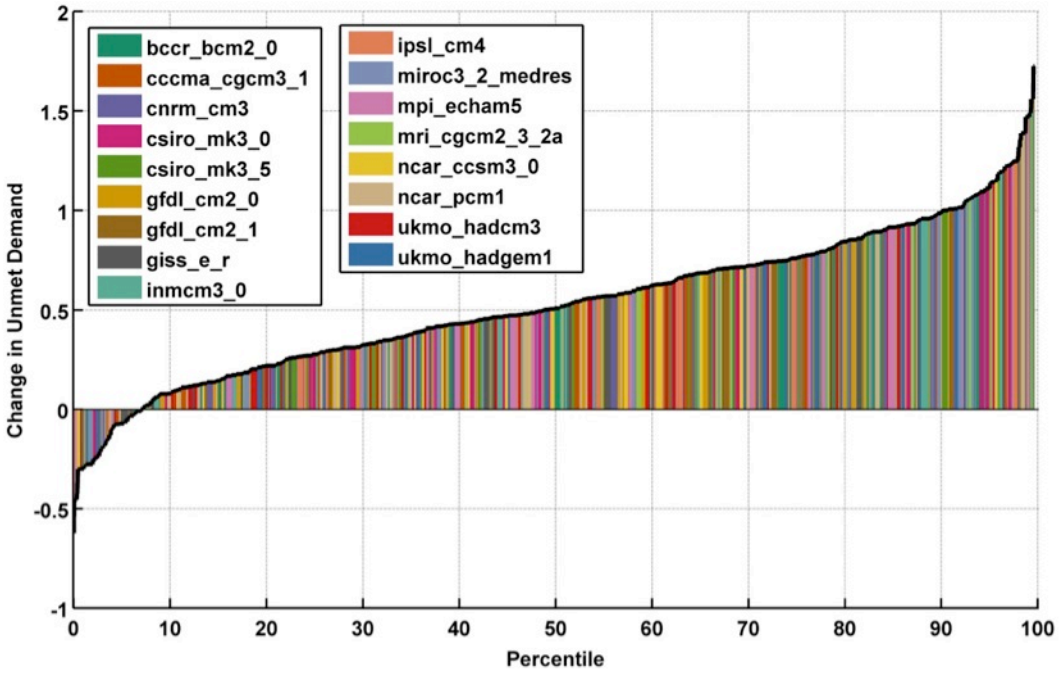

Figure B-3. Population weighted change in UWR (%) across the region for the *Just Climate* ensemble. The colors correspond to the GCM pattern used as denoted in the legend.

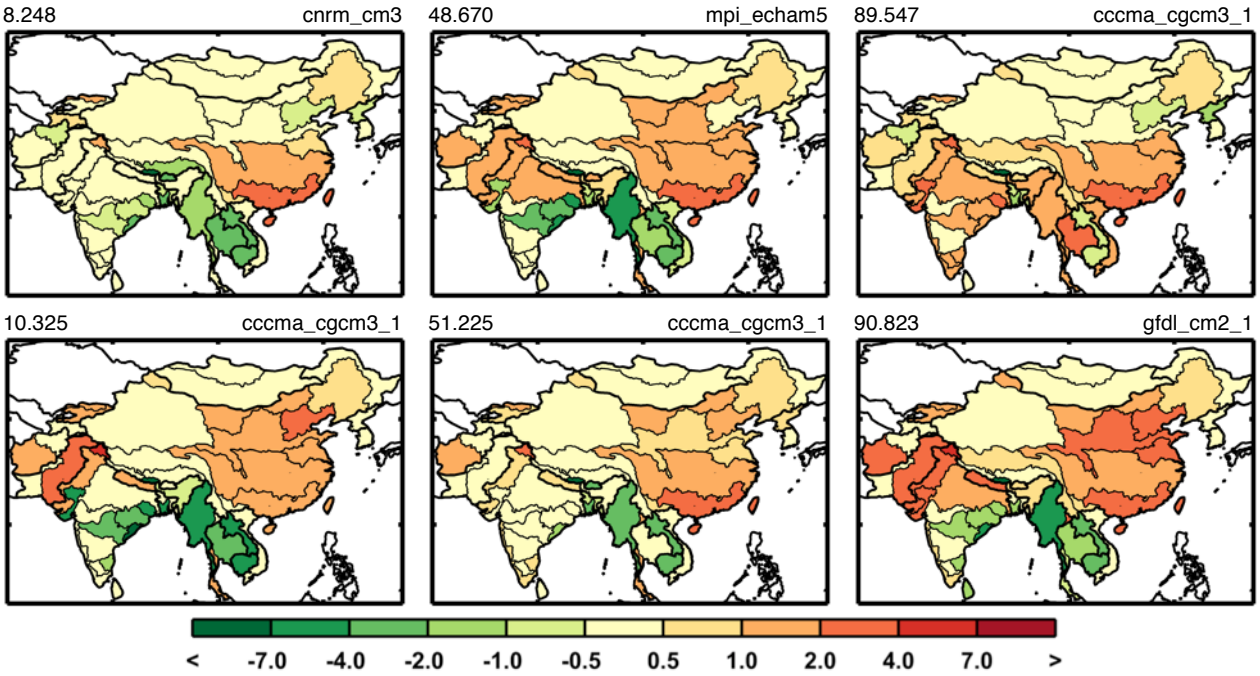

Figure B-4. UWR change for the *Just Climate* ensemble (in %) patterns around the 10th, 50th, and 90th percentile, two each, based on the mean UWR change for the region. Top label shows the percentile and GCM name.

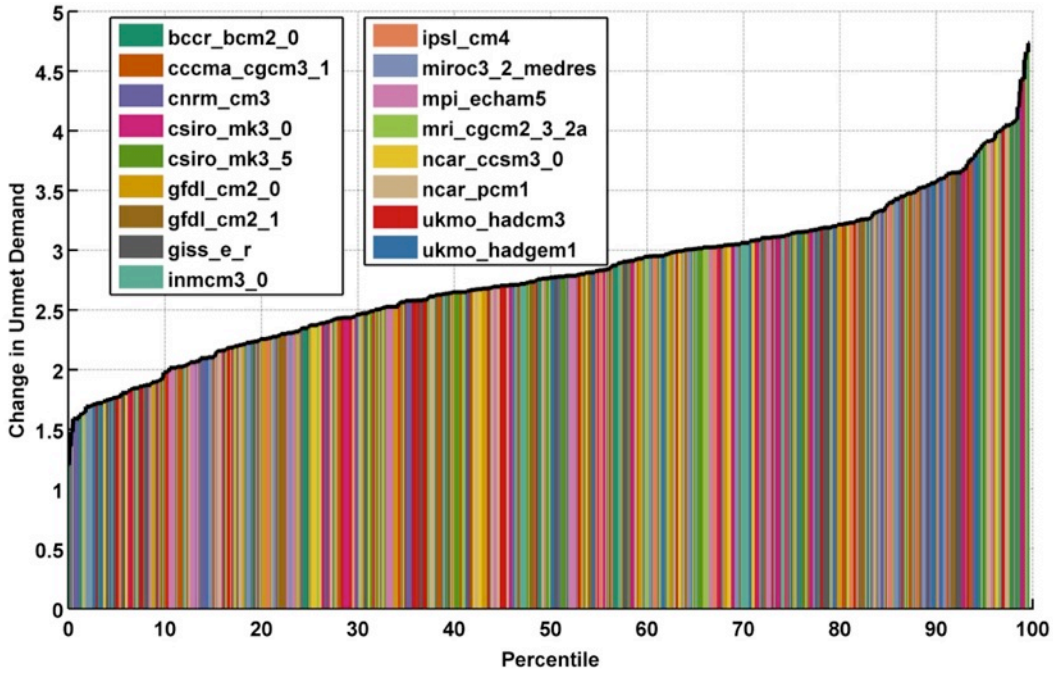

Figure B-5. Population weighted change in UWR (%) across the region for the *Climate and Growth* ensemble. The colors correspond to the GCM pattern used as denoted in the legend.

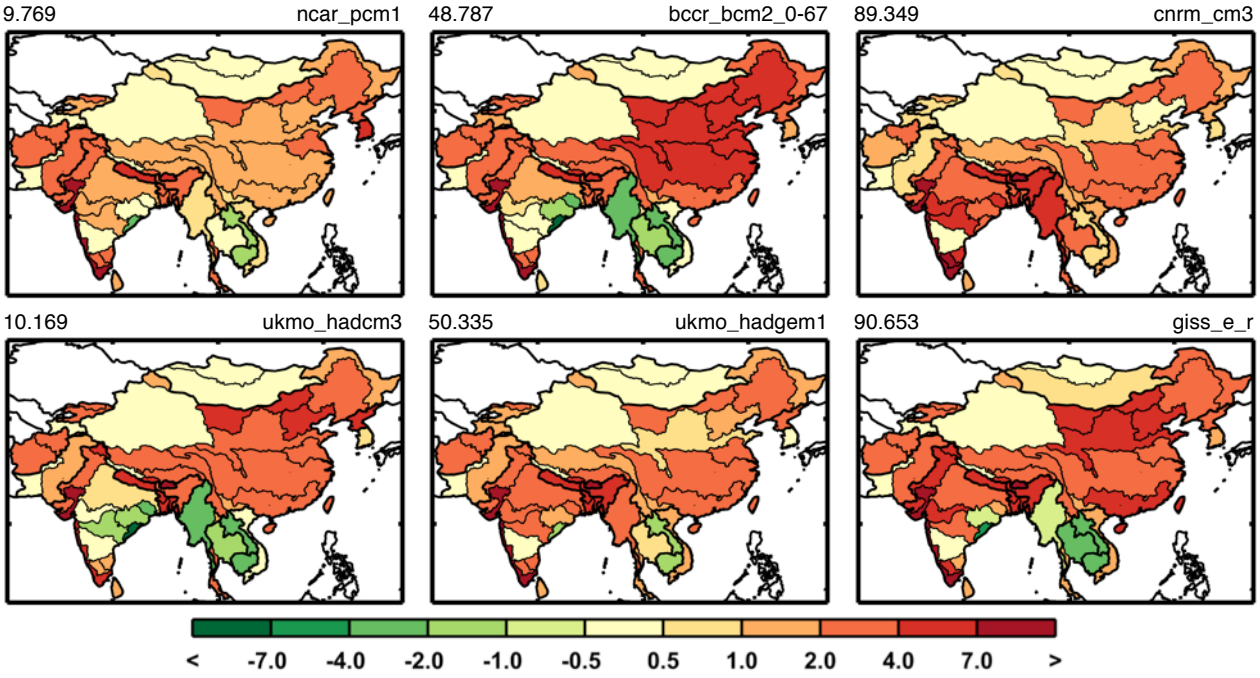

Figure B-6. UWR change for the *Climate and Growth* ensemble (in %) patterns around the 10th, 50th, and 90th percentile, two each, based on the mean UWR change for the region. Top label shows the percentile and GCM name.

APPENDIX C: WSI SINGLE METRIC AND MAPS

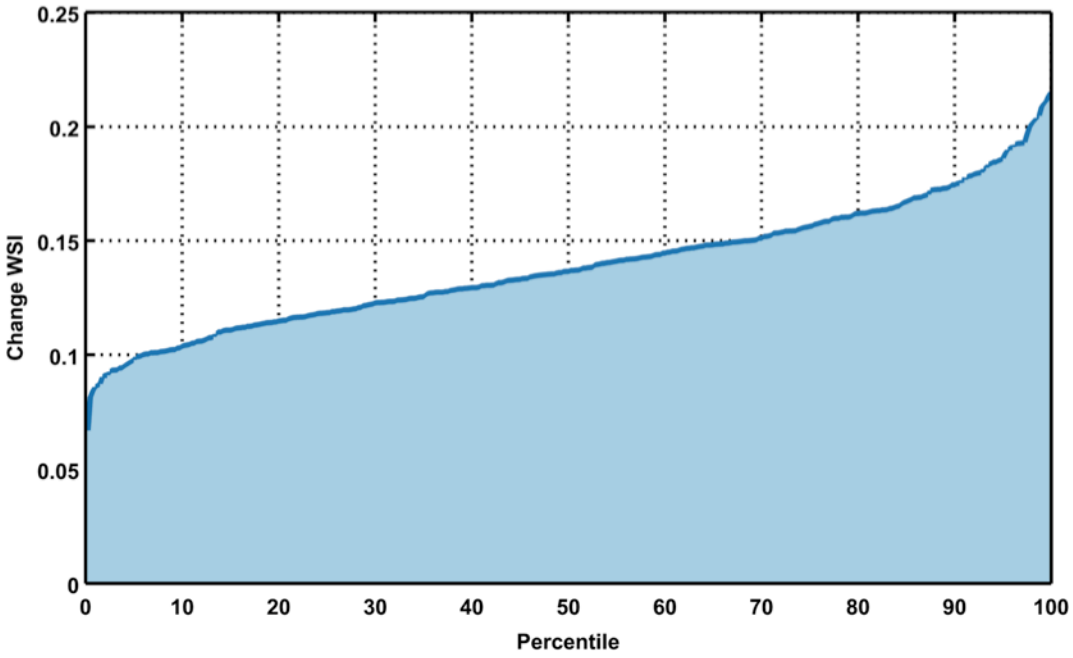

Figure C-1. Population weighted change in WSI (%) across the region for the *Just Growth* ensemble.

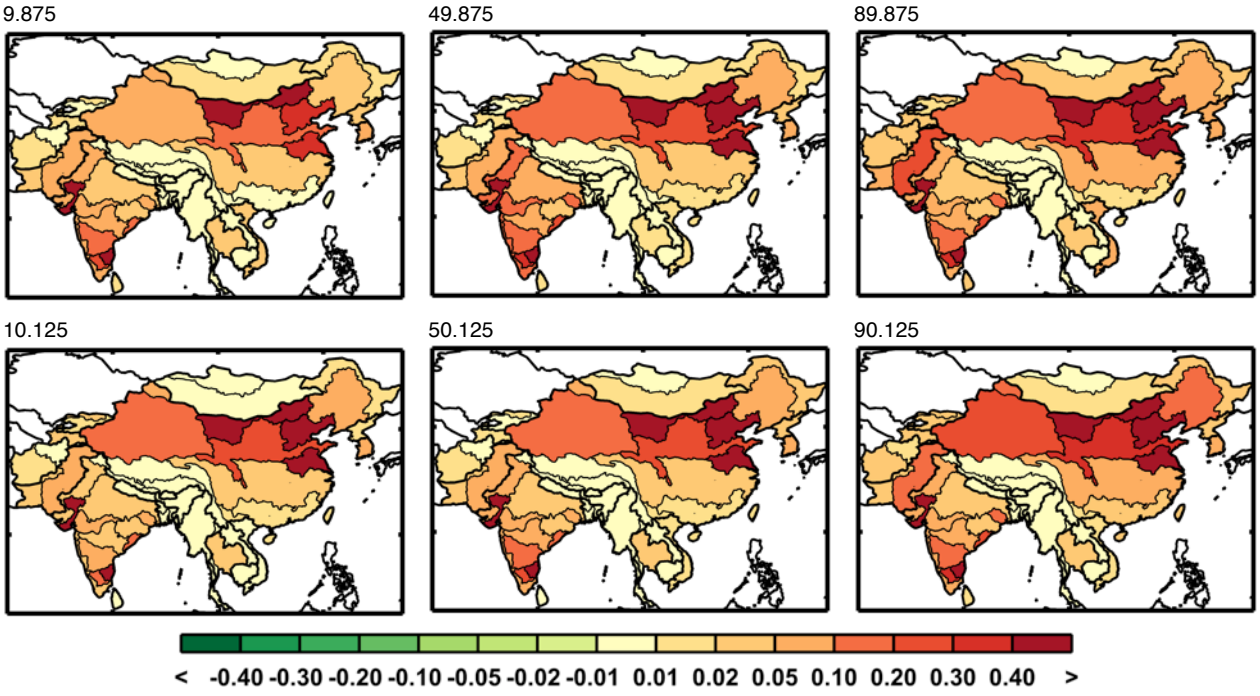

Figure C-2. WSI change for the *Just Growth* ensemble (unitless) patterns around the 10th, 50th, and 90th percentile, two each, based on the mean WSI change for the region. Top label shows the percentile

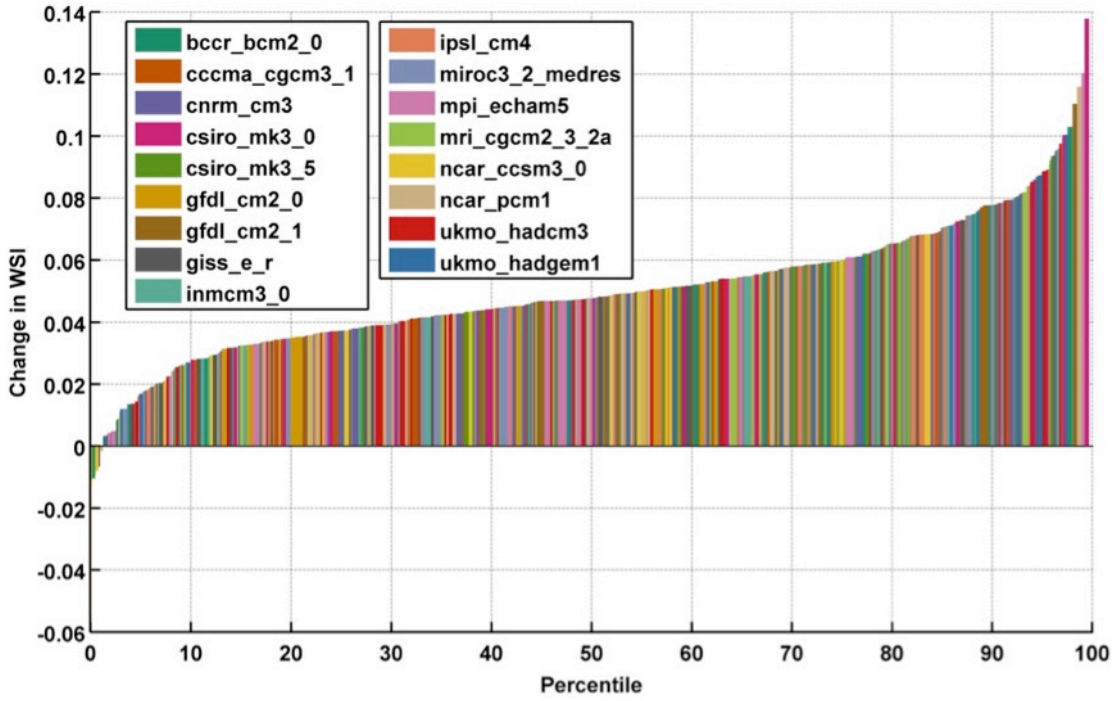

Figure C-3. Population weighted change in WSI across the region for the *Just Climate* ensemble. The colors correspond to the GCM pattern used as denoted in the legend.

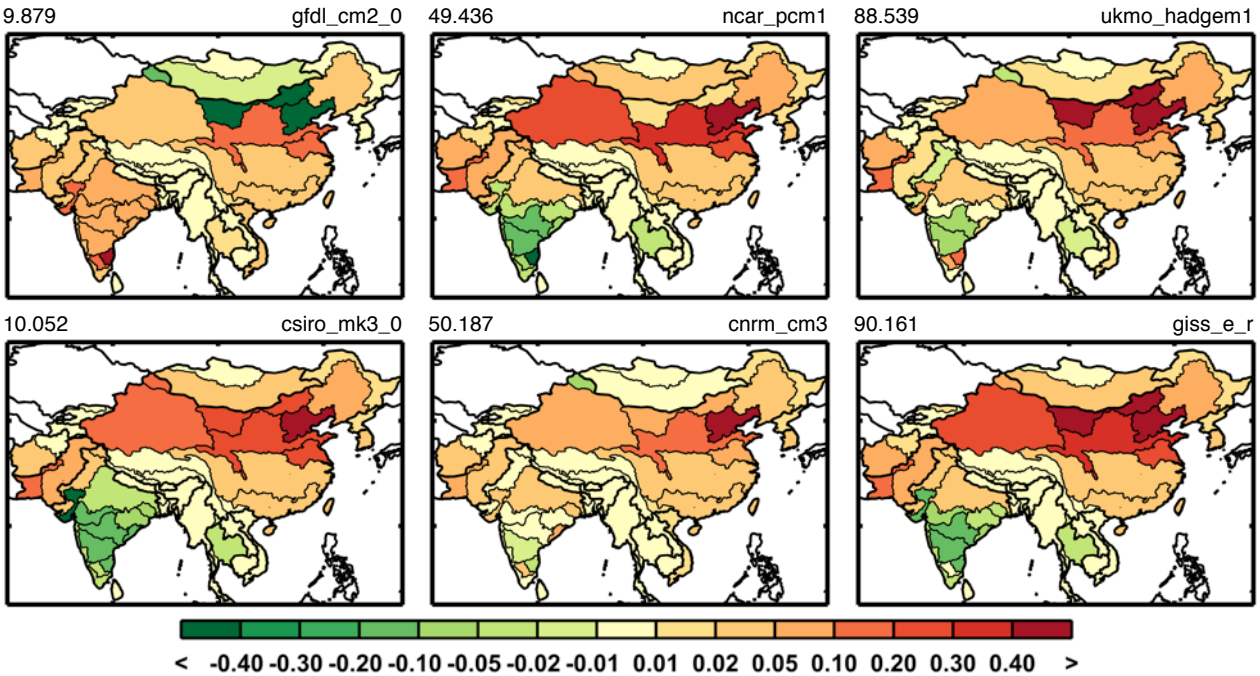

Figure C-4. WSI change for the *Just Climate* ensemble (unitless) patterns around the 10th, 50th, and 90th percentile, two each, based on the mean WSI change for the region. Top label shows the percentile and GCM name.

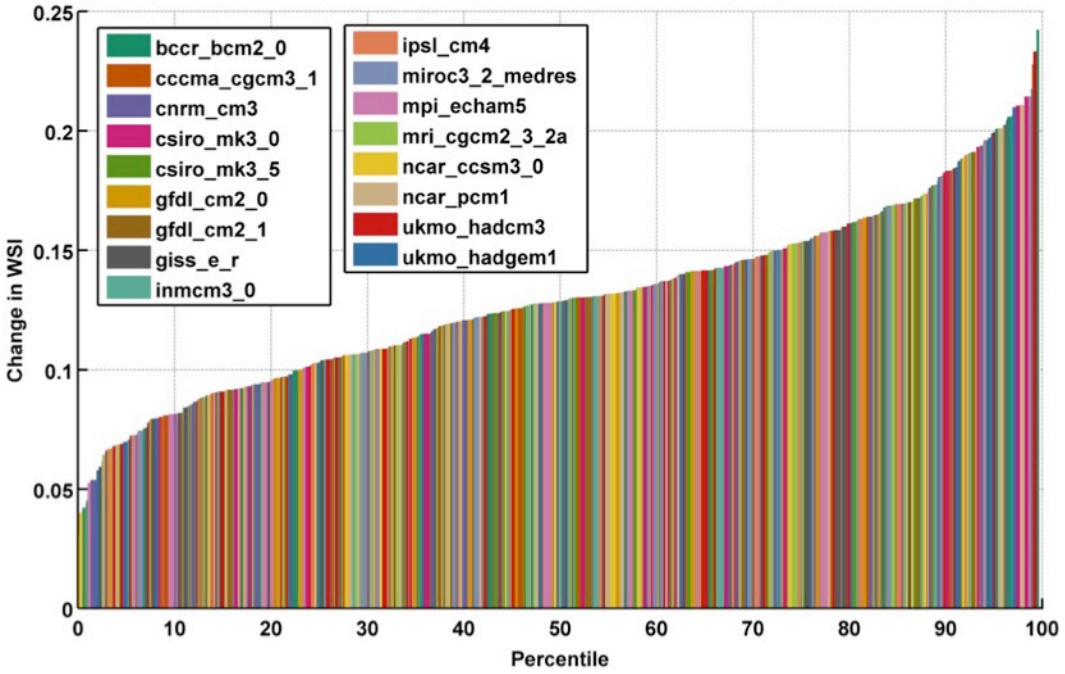

Figure C-5. Population weighted change in WSI across the region for the *Climate and Growth* ensemble. The colors correspond to the GCM pattern used as denoted in the legend.

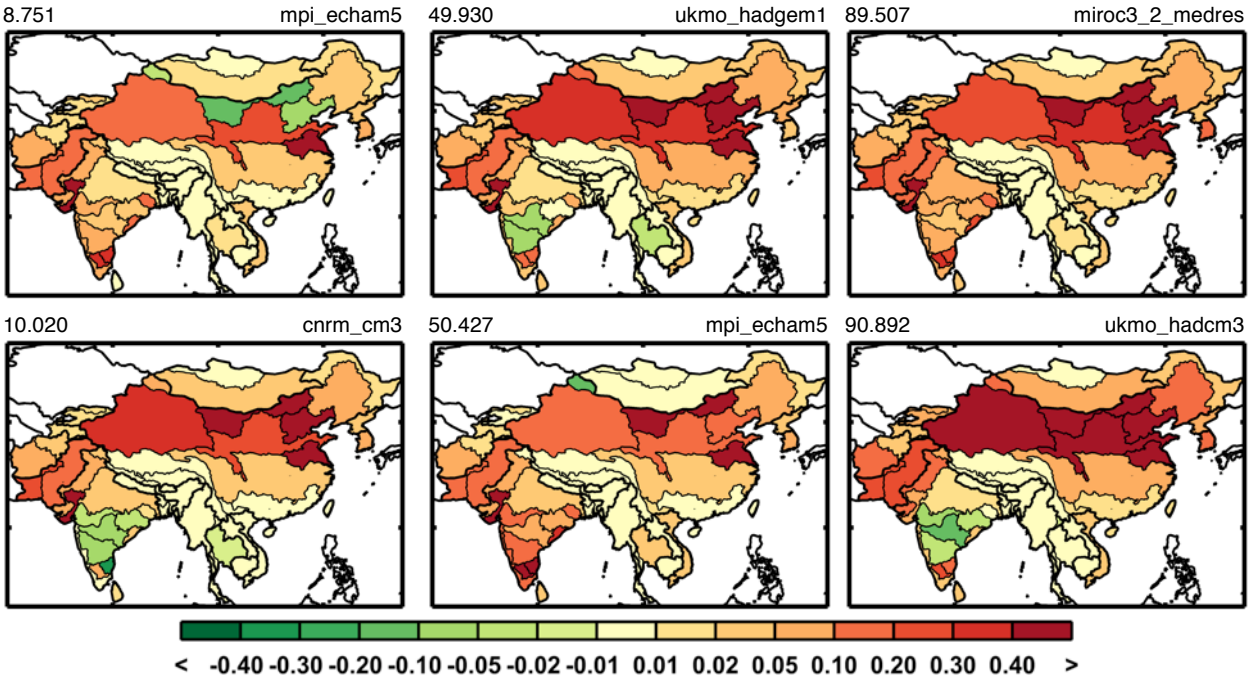

Figure C-6. WSI change for the *Climate and Growth* ensemble (unitless) patterns around the 10th, 50th, and 90th percentile, two each, based on the mean WSI change for the region. Top label shows the percentile and GCM name.

REPORT SERIES of the MIT Joint Program on the Science and Policy of Global Change

FOR THE COMPLETE LIST OF JOINT PROGRAM REPORTS: http://globalchange.mit.edu/pubs/all-reports.php

229. CLM-AG: An Agriculture Module for the Community Land Model version 3.5. *Gueneau et al.,* September 2012

230. Quantifying Regional Economic Impacts of CO_2 Intensity Targets in China. *Zhang et al.,* September 2012

231. The Future Energy and GHG Emissions Impact of Alternative Personal Transportation Pathways in China. *Kishimoto et al.,* September 2012

232. Will Economic Restructuring in China Reduce Trade Embodied CO_2 Emissions? *Qi et al.,* October 2012

233. Climate Co-benefits of Tighter SO_2 and NO_x Regulations in China. *Nam et al.,* October 2012

234. Shale Gas Production: *Potential versus Actual GHG Emissions*. *O'Sullivan and Paltsev,* November 2012

235. Non-Nuclear, Low-Carbon, or Both? *The Case of Taiwan*. *Chen,* December 2012

236. Modeling Water Resource Systems under Climate Change: *IGSM-WRS*. *Strzepek et al.,* December 2012

237. Analyzing the Regional Impact of a Fossil Energy Cap in China. *Zhang et al.,* January 2013

238. Market Cost of Renewable Jet Fuel Adoption in the United States. *Winchester et al.,* January 2013

239. Analysis of U.S. Water Resources under Climate Change. *Blanc et al.,* February 2013

240. Protection of Coastal Infrastructure under Rising Flood Risk. *Lickley et al.,* March 2013

241. Consumption-Based Adjustment of China's Emissions-Intensity Targets: *An Analysis of its Potential Economic Effects*. *Springmann et al.,* March 2013

242. The Energy and CO_2 Emissions Impact of Renewable Energy Development in China. *Zhang et al.,* April 2013

243. Integrated Economic and Climate Projections for Impact Assessment. *Paltsev et al.,* May 2013

244. A Framework for Modeling Uncertainty in Regional Climate Change. *Monier et al.,* May 2013

245. Climate Change Impacts on Extreme Events in the United States: An Uncertainty Analysis. *Monier and Gao,* May 2013

246. Probabilistic Projections of 21st Century Climate Change over Northern Eurasia. *Monier et al.,* July 2013

247. What GHG Concentration Targets are Reachable in this Century? *Paltsev et al.,* July 2013

248. The Energy and Economic Impacts of Expanding International Emissions Trading. *Qi et al.,* August 2013

249. Limited Sectoral Trading between the EU ETS and China. *Gavard et al.,* August 2013

250. The Association of Large-Scale Climate Variability and Teleconnections on Wind Resource over Europe and its Intermittency. *Kriesche and Schlosser,* September 2013

251. Regulatory Control of Vehicle and Power Plant Emissions: *How Effective and at What Cost?* *Paltsev et al.,* October 2013

252. Synergy between Pollution and Carbon Emissions Control: *Comparing China and the U.S.* *Nam et al.,* October 2013

253. An Analogue Approach to Identify Extreme Precipitation Events: *Evaluation and Application to CMIP5 Climate Models in the United States*. *Gao et al.* November 2013

254. The Future of Global Water Stress: *An Integrated Assessment*. *Schlosser et al.,* January 2014

255. The Mercury Game: *Evaluating a Negotiation Simulation that Teaches Students about Science–Policy Interactions*. *Stokes and Selin,* January 2014

256. The Potential Wind Power Resource in Australia: *A New Perspective*. *Hallgren et al.,* February 2014

257. Equity and Emissions Trading in China. *Zhang et al.,* February 2014

258. Characterization of the Wind Power Resource in Europe and its Intermittency. *Cosseron et al.,* March 2014

259. A Self-Consistent Method to Assess Air Quality Co-Benefits from US Climate Policies. *Saari et al.,* April 2014

260. Electricity Generation and Emissions Reduction Decisions under Policy Uncertainty: *A General Equilibrium Analysis*. *Morris et al.,* April 2014

261. An Integrated Assessment of China's Wind Energy Potential. *Zhang et al.,* April 2014

262. The China-in-Global Energy Model. *Qi et al.* May 2014

263. Markets versus Regulation: *The Efficiency and Distributional Impacts of U.S. Climate Policy Proposals*. *Rausch and Karplus,* May 2014

264. Expectations for a New Climate Agreement. *Jacoby and Chen,* August 2014

265. Coupling the High Complexity Land Surface Model ACASA to the Mesoscale Model WRF. *Xu et al.,* August 2014

266. The CO_2 Content of Consumption Across US Regions: *A Multi-Regional Input-Output (MRIO) Approach*. *Caron et al.,* August 2014

267. Carbon emissions in China: *How far can new efforts bend the curve?* *Zhang et al.,* October 2014

268. Characterization of the Solar Power Resource in Europe and Assessing Benefits of Co-Location with Wind Power Installations. *Bozonnat and Schlosser,* October 2014

269. A Framework for Analysis of the Uncertainty of Socioeconomic Growth and Climate Change on the Risk of Water Stress: *a Case Study in Asia*. *Fant et al.,* November 2014

Contact the Joint Program Office to request a copy. The Report Series is distributed at no charge.